horticulturae

MDPI

Article

Combining Vis-NIR Spectral Data and Multivariate Technique to Estimate Nutrient Contents in Peach Leaves

Jacson Hindersmann [1], Jean M. Moura-Bueno [1,*], Gustavo Brunetto [1], Tales Tiecher [2], William Natale [3], Eduarda Zanon Cargnin [1], Eduardo Dickel Ambrozzi [1], João Alex Tavares Pinto [1], Natália Adam [1], Gilberto Nava [4], Renan Navroski [5] and Fábio Joel Kochem Mallmann [1]

[1] Soil Science Department, Federal University of Santa Maria (UFSM), Santa Maria 97105-900, Brazil; jacsonjh7@gmail.com (J.H.); fabiojkmallmann@gmail.com (F.J.K.M.)
[2] Department of Soil Science, Center of Rural Science, Federal University of Rio Grande do Sul (UFRGS), Av. Bento Gonçalves 7712, Porto Alegre 91540-000, Brazil
[3] Brazilian Agricultural Research Corporation (EMBRAPA—Agroindustry Tropical), Fortaleza 60511-110, Brazil
[4] Embrapa Clima Temperado, Caixa Postal 403, Pelotas 96010-971, Brazil
[5] Federal University of Western Pará (UFOPA), Campus Juruti-PA, Santarem 68035-110, Brazil; navroski@outlook.com
* Correspondence: bueno.jean1@gmail.com; Tel.: +55-(55)-9-9666-9855

Abstract

Peach tree (*Prunus persica* L. Batsch) is a fruit species of great economic importance worldwide. Thousands of chemical leaf analyses are performed on a yearly basis to support decision-making about fertilizer application. However, traditional methods to determine nutrient content in plant tissue require a mix of strong acids, besides being time-consuming and generating polluting waste. Visible (Vis) and near-infrared (NIR) spectroscopy combined with multivariate techniques emerges as a potential solution to overcome limitations of traditional chemical analyses. The aim of the present study is to combine Vis-NIR spectral data and multivariate techniques to test strategies for the development of models to estimate nutrient content in peach leaves. The study estimated N, P, K, Ca, Mg, S, B, Cu, Fe, Mn, and Zn content in the leaves of peach trees grown in two locations, namely: *Pelotas* and *Pinto Bandeira*, in Southern Brazil. Therefore, local and regional scale prediction models were developed by combining preprocessed Vis-NIR spectral data to both Savitzky–Golay first-derivative (SGD1d) and partial least squares regression (PLSR) multivariate technique. Most of the proposed prediction models showed average accuracy ($R^2 \geq 0.50$ and <0.75, RPIQ ≥ 1.9 and <3.0). The local-1 'PB' model showed higher nutrient prediction accuracy than the regional 'PB + Pelotas' model and the local-2 'Pelotas' model. Estimates on nutrient content in peach tree leaves subjected to local, local-1 'PB' and local-2 'Pelotas' models fed with data collected in the same site showed better performance than calculations based on data from other sites and/or regions. Finally, the current study allowed making updates in the refinement of more sustainable techniques to set nutrient content.

Keywords: *Prunus persica*; Vis-NIR spectroscopy; prediction models scaling; sustainable techniques; leaf spectral library

Academic Editor: Adriana Guerreiro and Jianwei Qin

Received: 11 August 2025
Revised: 05 February 2026
Accepted: 27 February 2026
Published: 2 March 2026

1. Introduction

Peach tree (*Prunus persica* L. Batsch) is a fruit species native to China, which is the country accounting for the largest global production of this crop with more than 17 million tons of peaches in 2023 [1]. Peach cultivation covers 2.447,827 hectares worldwide, and it resulted in a total production of 44,594,372 tons in the same year [1]. According to IBGE data, this crop covered 15,627 hectares in Brazil in 2023, with a total production of 200,710 tons of peaches and gross production close to R$646 million. Rio Grande do Sul State is its main producer, with 130,823 tons, and it is followed by Santa Catarina (17,978 t) and São Paulo (29,467 t) states.

Although peaches are the third most important temperate fruit species in Brazil, since it is only behind grapes and apples, the national average productivity of this crop remains low (12,844 kg ha^{-1}) [2,3] compared to other traditionally producing countries such as Italy (18,000 kg ha^{-1}), China (19,400 kg ha^{-1}), United States (20,650 kg ha^{-1}), and Chile (21,600 kg ha^{-1}) [3]. This production limitation can be partly related to proper plant nutrition because tropical and subtropical soils do not always provide nutrients in adequate amounts to meet this crop's requirements [4], a fact that implies increasingly improving production systems with emphasis on quality and yield.

Currently, decision-making on fertilization recommendations for fruit species exclusively relies on reports about soil and plant tissue (leaves) nutrient content analysis. Accordingly, thousands of chemical analyses are performed on a yearly basis for diagnostic and fertilizer recommendation purposes. However, methods traditionally adopted to set nutrient content in leaves require wet chemistry analysis based on methodologies that use a mix of strong acids (sulfuric acid H_2SO_2, nitric acid HNO_3 and perchloric acid $HClO_4$); however, these methodologies are time-consuming, laborious tasks that generate polluting waste—if it is not properly treated [5–7].

Thus, proposing more sustainable tissue analysis techniques to enable fast, nondestructive and low-cost measurements to assess nutrient content in leaves is a challenge, mainly when it comes to reducing chemical waste generation. Visible (Vis) and near-infrared (NIR) spectroscopy techniques have merged, and they are based on proximal sensing supported by the use of hyperspectral sensors. Recent studies show that Vis-NIR spectroscopy in combination with multivariate technique methods has the potential to quickly and accurately quantify nutrient content in plant tissue (leaves) of both fruit trees and other plant species [5–13]. This technique is based on previously calibrated models and is adopted to predict the content of nutrients such as nitrogen (N), phosphorus (P), potassium (K), calcium (Ca), magnesium (Mg), as well as some micronutrients in leaves by only finding one spectrum per sample. Thus, the Vis-NIR + multivariate technique combination is pointed out as a likely solution to overcome limitations of traditional chemical analyses conducted to determine nutrients in leaves.

The global use of Vis-NIR spectroscopy to estimate tissue nutrients remains incipient, mainly in fruit species like peach trees. Lack of leaf spectra databases, also known as leaf spectral libraries, is one of the reasons justifying this limitation. Furthermore, this technique remains limited to predict accuracy, and it highlights the need for further studies and research aimed at developing strategies to calibrate prediction models in order to make their estimates closer to those derived from traditional tissue analysis methods (wet chemistry). Recent studies have pointed out that the estimates' low/medium accuracy is related to the scale/scope of regional and local spectral libraries, to the machine learning type adopted to calibrate the prediction models and to intrinsic nutrient features (e.g., standard deviation) of the analyzed tissues. Thus, sample heterogeneity can lead to bias in tissue nutrient content estimates in studies based on Vis-NIR spectroscopy [10–15], and it highlights the need for research aimed at regionalized strategies to solve and/or minimize this problem. Calibrating specific local models, for example, can be a strategy for

https://doi.org/10.3390/horticulturae12030296

specific locations or cultivars. This strategy is based on the hypothesis that local models present higher nutrient estimate accuracy than regional models.

Thus, this study aimed to develop and evaluate prediction models for nutrient contents in peach leaves from Southern Brazil using Vis-NIR spectroscopy and multivariate techniques based on local and regional spectral libraries, as well as to discuss the intrinsic factors of the dataset that influence the performance of the models and their applicability.

2. Materials and Methods

2.1. Study Sites

Nutrient content estimates for peach tree leaves were performed based on a database (DB) of leaf samples collected from orchards distributed in two municipalities in Rio Grande do Sul State, namely, Pinto Bandeira (PB) (n = 146—Northeastern RS State) and Pelotas (n = 390—Southeastern RS State), and it totaled 536 observations from three cultivars, altogether ['PS 10711' crown (n = 146), 'Maciel' crown (n = 210) and 'Granada' crown (n = 180)]. Results derived from leaf samples of fruiting branches collected in two different harvest seasons (November and December 2022/2023 and 2023/2024) in Pinto Bandeira and in three different harvests (2017/2018, 2018/2019, 2019/2020) in Pelotas.

Pinto Bandeira DB regards samples collected from full-production plants from commercial peach farms' orchards intended for fresh consumption. Pelotas DB mostly resulted from samples collected from sites where peach trees are grown for industrial use.

2.2. Soil Features in the Study Sites

Pinto Bandeira municipality is dominated by four main soil classes: Haplic Chernosol and Litholic Neosol, which are often found in the lower elevations, and Grayish Argisol and Haplic Cambisol, which occur in the upper elevations. All of them belong to the basaltic/rhyodacite origin class [16]. Soil classes most often found in the Pelotas region are classified as Argisols and Planossolos; the red–yellow Argisol class is the most representative in sites where fruit trees, such as peaches, are grown [17]. Soil physicochemical features in the study sites are described in Table S1.

2.3. Leaf Sampling

Plants were randomly sampled in each orchard. Ill or blemished plants and leaves were avoided. One hundred complete leaves (blade + petiole) were collected from the mid-section of the branches produced over the year on different plant sides. Leaves were collected from peach trees in November and December (from 13 to 15 weeks after full blooming) [18,19].

2.4. Chemical Analysis of Leaf Nutrients

Total nitrogen (N), phosphorus (P), potassium (K), calcium (Ca), magnesium (Mg), sulfur (S) (except for the Pelotas database), boron (B), copper (Cu), iron (Ferro), manganese (Mn) and zinc (Zn) contents in the leaf samples were analyzed through standard procedures, according to methodologies proposed by Tedesco [20], Embrapa [21] and Embrapa [22].

A tissue subsample was subjected to sulfuric digestion (H_2SO_4 + H_2O_2) [20] in a digestion block (Tecnal, Micro 42, Piracicaba, Brazil). Subsequently, the digestion extract was distilled in a micro-Kjeldahl steam distiller (TE-0363, Tecnal, Piracicaba, Brazil) and titrated in 0.025 mol L^{-1} sulfuric acid for total N determination.

Another tissue part was subjected to nitroperchloric digestion (HNO_3 + $HClO_4$) to determine total P, K, Ca, Mg, S, Cu, Zn, Fe, and Mn contents [22]. After digestion, total P was quantified by colorimetric analysis using the molybdenum blue method, with absorbance measured at 882 nm in a UV–visible spectrophotometer (SF325NM, Bel Engineering, Monza, Italy), according to the Murphy & Riley methodology [23]. Total K content was determined in a

flame photometer (DM62, Digimed, São Paulo, Brazil). The concentrations of Ca, Mg, Cu, Zn, Fe, and Mn were determined by atomic absorption spectrophotometry (AAnalyst 200, PerkinElmer, Singapore) using element-specific hollow cathode lamps and calibration curves prepared from analytical-grade standard solutions [20]. Total S was determined in the $BaCl_2$-gelatin method, based on the formation of barium sulfate ($BaSO_4$) precipitate, with absorbance measured at 420 nm in a UV–visible spectrophotometer at 420 nm (SF325NM, Bel Engineering, Monza, Italy), according to the Tedesco methodology [20]. The DB of samples belonging to cultivar 'Maciel' did not provide S values. Another tissue subsample was taken to the muffle, and the resulting ash was solubilized for subsequent analysis. Boron content was determined by colorimetric spectrophotometry using the azomethine-H method, with absorbance measured at 435 nm in a UV–visible spectrophotometer (SF325NM, Bel Engineering, Monza, Italy), according to the methodology described by [21].

2.5. Collecting Vis-NIR Spectroscopy and Spectral Preprocessing Data

The collected leaves were washed in distilled water and dried in an oven under forced air circulation at 65 °C until reaching constant dry mass, in a laboratory environment. The dried leaves were ground in a Willey mill until their particles were smaller than 2 mm; they were reserved for spectroscopic and chemical analyses.

Leaf samples' spectral reflectance reading was performed in a FildSpec 4 spectroradiometer (Analytical Spectral Devices, Boulder, USA). Peach leaf samples' spectral reflectance reading was carried out with the same samples used for nutrient determination based on chemical methods by using approximately 10 cm^3 of leaves (dry and ground tissue) per sample, arranged in a Petri dish. Each reading represents the spectral response of a composite leaf sample collected in the field, composed of 100 fully developed leaves (blade + petiole), following the sampling procedure described in Section 2.3.

Leaf nutrient content data collected through the wet chemistry method and leaf tissue spectral reflectance (raw data—RAW; Figure S1) were organized into a peach leaf spectral library—LSL, which comprised 536 samples (Figure S2). The SGD1d preprocessing [24] was applied to raw (RAW) leaf reflectance spectral data at the 350–2500 nm range (Figure 1) to remove physical variability due to light scattering, as well as to emphasize features of interest across the spectrum. The first derivative used a first-order polynomial with a 9 mm moving window (Figure 1). This technique is widely used to remove baseline shifts and to highlight spectral features of interest [25]. It has shown better leaf nutrient prediction results [12]. All spectra preprocessing was performed in the *prospectr* package - version 0.2.8 [26] of the R software [27].

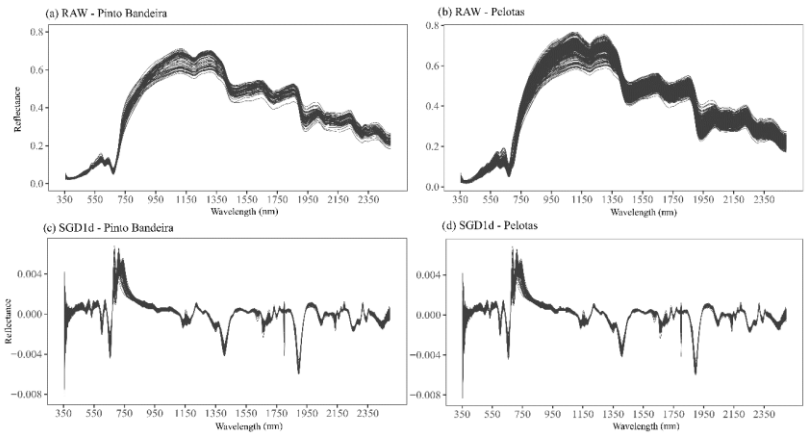

Figure 1. Spectral curves of leaf samples from peach cultivars grown in *Pinto Bandeira* and *Pelotas* regions without pre-processing (RAW) (**a**,**b**), pre-processed in Savitzky–Golay 1st derivative (SGD1d) (**c**,**d**).

The combination of spectral and nutritional data resulted in three peach leaf spectral libraries (LSL), hereinafter referred to as LSL local-1 (data of *Pinto Bandeira*; n = 146), LSL local-2 (data of *Pelotas*; n = 390) and regional LSL (data of *Pinto Bandeira* + *Pelotas*; n = 539).

2.6. Statistical Analysis

Descriptive statistics were performed to generate histograms aimed at featuring variations in nutrient content in peach leaves. Predicted spectral values quantitative analysis was conducted through principal component analysis (PCA) in order to identify how the information from the original variables (nutrient content in leaf and spectral data) is contained in the CPs, and similarity/dissimilarity in 'Pinto Bandeira' and 'Pelotas' databases.

2.7. Calibration and Assessment of Leaf Nutrient Content Prediction Models

Two calibration strategies were implemented and compared. The first one concerned calibrating a model called 'regional model' (Model 1) based on regional LSL (data of *Pinto Bandeira* + *Pelotas*), which comprised 536 samples (Figure S2).

The second approach regarded calibrating local models from regional LSL subdivision into local sub-libraries, namely: local-1 model (Model 2: data from *Pinto Bandeira*, n = 146) and local-2 model (Model 3: data from Pelotas, n = 390) (Figure S2).

The prediction models were calibrated through the multivariate statistical method of partial least squares regression (PLSR). This model was chosen because the literature often points out that the highest prediction accuracy is achieved through this method when it is calibrated based on Vis-NIR spectroscopy data [13,28]. This method is used to calibrate predictive models when the number of predictor variables is too large and collinear. Therefore, it stands out among multivariate calibration methods substantiated by spectral data; it is the most widely used for the quantitative analysis of plant tissue reflectance spectra [13,28,29]. PLSR is a parametric technique based on linear correlations between predictor variable projections and the response variable on a set of latent variables and corresponding scores used to minimize data dimensionality (principal components). The input vector (X) for the PLSR models consisted of preprocessed leaf reflectance values at all selected wavelengths, which were mean-centered and scaled prior to model calibration. Nutrient concentrations obtained from foliar chemical analyses were used as response variables (Y). Latent variables were extracted by maximizing the covariance between X and Y, enabling dimensionality reduction while retaining the most relevant spectral information for nutrient prediction [29]. The model's calibration process was conducted in the 'caret' package [30] of the R software [26].

Model calibration was performed by using preprocessed spectral data through the Savitzky–Golay first derivative (SGD1d) technique. Prediction models for leaf macro- and micronutrient contents were calibrated, resulting in a total of 31 distinct models: 11 models for the LSL local-1 'PB' dataset, covering 11 elements (N, P, K, Ca, Mg, S, B, Cu, Fe, Mn, and Zn), and 20 models for the LSL local-2 'Pel' and LSL regional, covering 10 elements (N, P, K, Ca, Mg, B, Cu, Fe, Mn, and Zn), totaling 31 models (Figure S2). Each LSL (regional, local-1, local-2) was randomly partitioned into two subsets through the Kennard–Stone (KS) method [31] to calibrate the three models—calibration with 70% of the samples and validation with the remaining 30% of them. The Levene test at significance level $\alpha = 0.05$ was run to assess variance homogeneity between calibration and validation subsets.

Cross-validation was used to adjust the models' "ncomp" parameter (number of principal components used by PLSR) by adopting a random division into 10 groups (10-fold) [32]. In this step, the models were calibrated using 100 independent replicates, allowing a consistent assessment of the variance explained in Y in relation to the variance explained in X. This procedure ensured model parsimony, robustness, and generalizability, particularly in datasets with a limited number of observations and high dimensionality and multicollinearity among predictor variables. Moreover, it helped to prevent overfitting associated with the excessive inclusion of latent variables, which may lead to good calibration performance but poor predictive ability when applied to independent data. In addition to this, after calibration, each model was validated based on the validation samples (30% data from each LSL) to assess the models' ability to predict leaf nutrient content in external samples after the calibration stage was over (Figure S2).

The following statistics were used to assess the model's performance and accuracy: coefficient of determination (R^2) (Equation (1)), root mean square prediction error (RMSE) (Equation (2)), mean absolute error (MAE) (Equation (3)) and ratio of performance to interquartile distance (RPIQ) (Equation (4)) (Figure S2) [14,33].

$$R^2 = \frac{\sum_{i=1}^{n}(\hat{y}_i - \bar{y}_i)^2}{\sum_{i=1}^{n}(y_i - \bar{y}_i)^2} \quad (1)$$

$$RMSE = \sqrt{\frac{1}{n}\sum_{i=1}^{n}(\hat{y}_i - y_i)^2} \quad (2)$$

$$MAE = \frac{1}{n}\sum_{i=1}^{N}(\hat{y}_i - y_i) \quad (3)$$

$$RPIQ = \frac{(Q3 - Q1)}{RMSE} \quad (4)$$

wherein $\hat{y}$ = predicted value; $\bar{y}$ = mean observed value; y = observed values; n = number of samples with i = 1, 2,…, n; $Q1$ = 25% of the samples; $Q3$ = 75% of the samples; and interquartile distance = $Q3 - Q1$ represent the interval accounting for 50% of the population around the median.

These statistical parameters were applied to assess the quality of prediction models at the calibration and validation stages. These parameters are very important to highlight the proposed model's ability to predict the content of a given nutrient by taking the content determined through the traditional method (wet chemistry, for example) as a reference. Parameter R^2 measures the quality of fit, which represents the explained variability level accounted for by the model. An R^2 close to 0 is indicative of an association between predicted spectral values and measured laboratory values, whereas an R^2 close to 1 points towards a close association between predicted and measured values [33]. RPIQ considers the prediction error in comparison to variations in the measured values [33]. RMSE assesses differences between predicted and measured values, and quantifies accuracy by comparing the prediction errors of different models [33]. MAE is the sum of absolute error values divided by the number of observations, and it represents the mean differences between the model's predicted and measured data. In other words, MAE quantifies how close the predicted values are to the measured reference values by giving less weight to errors in comparison to RMSE [33].

https://doi.org/10.3390/horticulturae12030296

Overall, a robust model should have high R^2 and RPIQ, and low RMSE and MAE [14,33]. R^2 is the most popular modeling performance statistic to allow comparing results across studies [33]; this is why it is one of the most widely used parameters. The model quality classification suggested by Johnson [34] was adopted for interpretation purposes, wherein $R^2 \geq 0.75$ highlights models with a high prediction level; $R^2 \geq 0.50$ and < 0.75 point out models with a medium prediction level; and $R^2 < 0.50$ are the non-recommended models. The classification proposed by Chang [35] and Veum [36] was used to interpret the quality of models by using parameters, according to which models in category A present a high reliability level RPIQ ≥ 3.0. Subsequently, one finds models in category B, with mean reliability RPIQ ≥ 1.9 and < 3.0, and models in category C, with low reliability RPIQ ≥ 1.5 and < 1.9. All multivariate statistical analyses were performed in R software [26].

The nutritional values determined by the reference method (wet chemistry) and those estimated by the Vis–NIR models were classified according to nutrient sufficiency range (SR) values established for peach cultivation in Southern Brazil (Table S2) [37], in order to assess the applicability of the nutrient estimates derived from the developed prediction models. The accuracy percentage of the samples with nutrient values estimated through Vis-NIR was calculated in comparison to the classification of values derived from the reference method (wet chemistry) based on the interpretation of nutrient values in each class. The values were classified into three classes, namely: below SR; adequate, within the SR limit; and above SR. This classification allowed us to find the accuracy percentage of the estimates for each model: local-1 'PB', local-2 'Pelotas', and regional 'PB + Pelotas'. Models achieving more than 80% accuracy were considered suitable for result interpretation purposes, aiming at the nutritional diagnosis of the peach crop.

3. Results

3.1. Descriptive Analysis of the Database

According to the descriptive statistics, there are different amplitudes in the content of the assessed macronutrients based on the three adopted databases (DB), namely: PB, Pelotas and PB + Pel (Figure 2). N and K contents in peach leaves showed a wide range of values. The greatest variability and standard deviation (SD) values were observed in the 'Pelotas' database (DB), with N ranging from 14.74 to 40.84 g kg^{-1} (SD = 5.00 g kg^{-1}) and K from 8.02 to 32.66 g kg^{-1} (SD = 3.34 g kg^{-1}). In contrast, the lowest variability was recorded in the 'PB' DB, with N ranging from 22.62 to 35.54 g kg^{-1} (SD = 2.83 g kg^{-1}) and K from 14.61 to 30.81 g kg^{-1} (SD = 3.42 g kg^{-1} (Figure 2a,c).

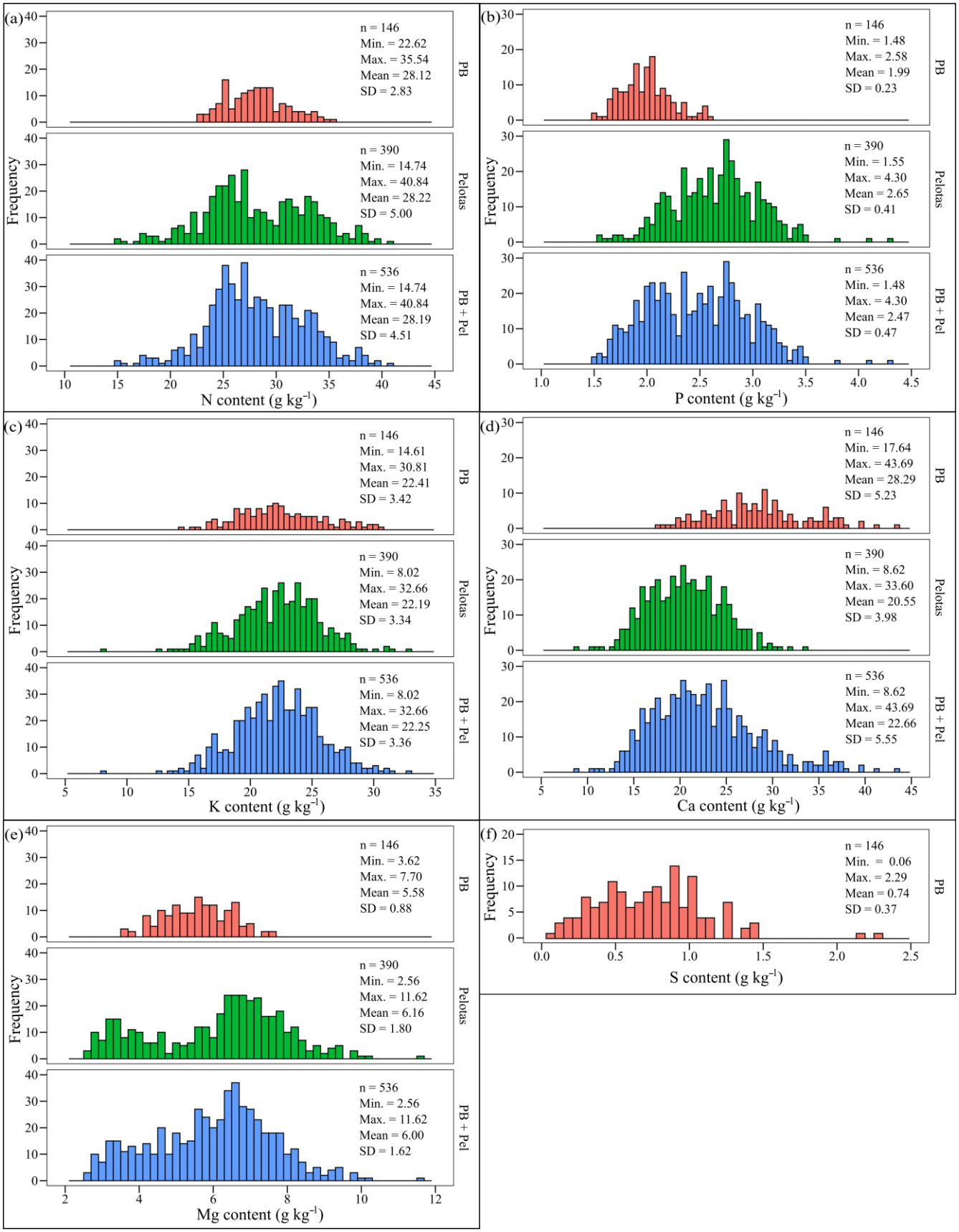

Figure 2. Frequency histograms plotted for data on the contents of macronutrients N (**a**), P (**b**), K (**c**), Ca (**d**), Mg (**e**) and S (**f**) in peach cultivars grown in 'Pinto Bandeira' and 'Pelotas', Southern Brazil. PB = Pinto Bandira; Pel = Pelotas; n = number of samples in the sample set; Min = minimum; Max = maximum; SD = standard deviation.

https://doi.org/10.3390/horticulturae12030296

P and Mg contents in peach leaves showed a smaller range in comparison to other macronutrients, except for S, which accounted for the smallest range in comparison to other macronutrients (0.06 to 2.29 g kg^{-1}, SD 0.37 g kg^{-1}) (Figure 2b,e,f). The widest P and Mg content ranges were observed for BD 'Pelotas' (1.55 to 4.30 g kg^{-1}, SD 0.41 g kg^{-1}; and 2.56 to 11.62 g kg^{-1}, SD 1.80 g kg^{-1}, respectively), and the smallest range was recorded for BD 'PB' (1.48 to 2.58 g kg^{-1}, SD 0.23 g kg^{-1}; and 3.62 to 7.70 g kg^{-1}, SD 0.88 g kg^{-1}, respectively) (Figure 2b,e).

Ca content in peach leaves showed a wide range of values in BD 'PB' and 'Pelotas'; the widest range was observed for BD 'PB' (17.64 to 43.69 g kg^{-1}, SD 5.23 g kg^{-1}) and smallest rage was recorded for BD 'Pelotas' (8.62 to 33.60 g kg^{-1}, SD 3.98 g kg^{-1}) (Figure 2d).

The micronutrients also presented different content amplitudes in the three assessed BD: PB, Pelotas and PB + Pel (Figure 3). B and Cu contents presented the smallest amplitude in comparison to the other micronutrients (Fe, Mn, Zn) (Figure 3a–e).

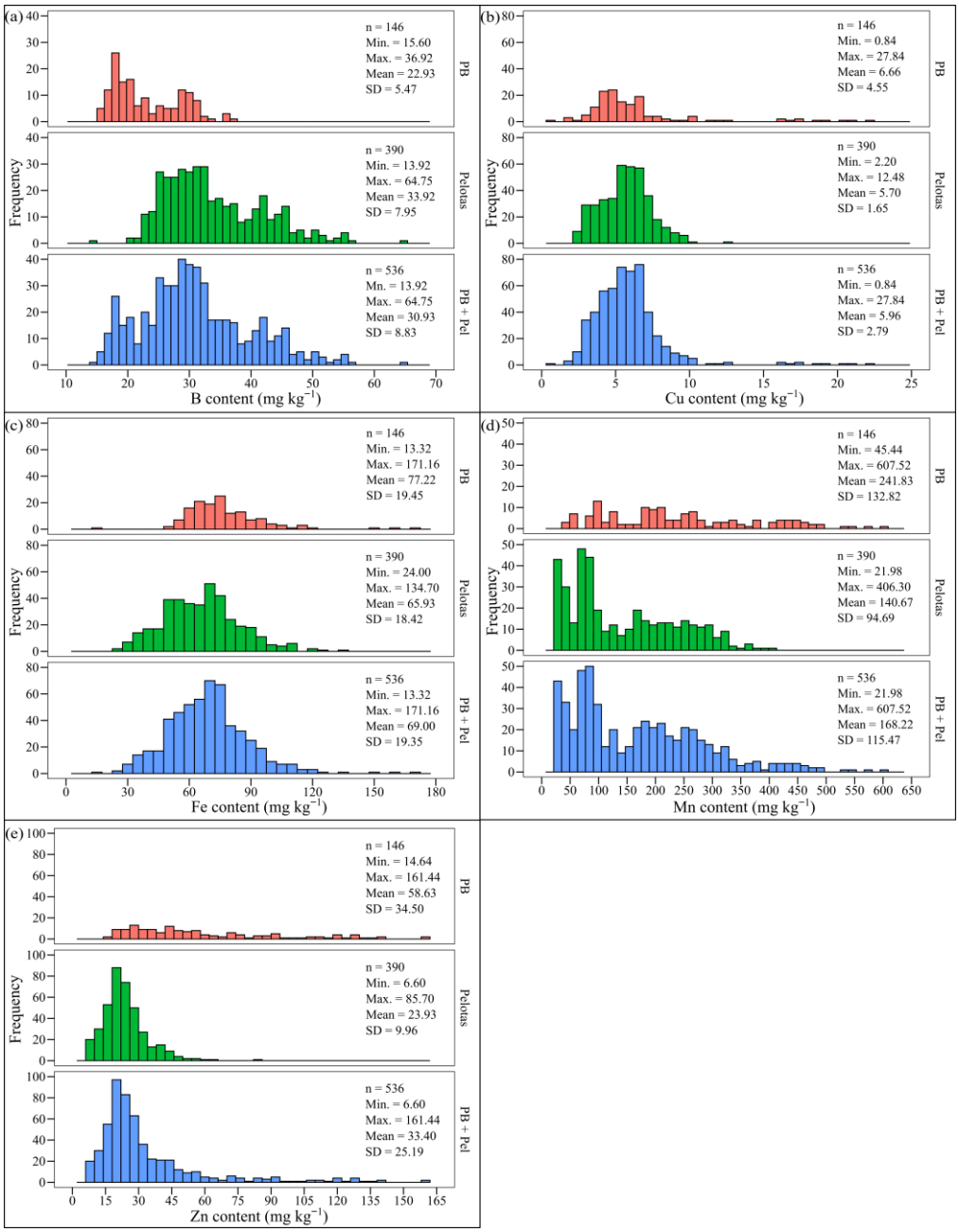

Figure 3. Frequency histograms plotted for data on the content of micronutrients B (**a**), Cu (**b**), Fe (**c**), Mn (**d**) and Zn (**e**) in peach cultivars grown in Pinto Bandeira and Pelotas, Southern Brazil. PB =

Pinto Bandeira; Pel = Pelotas; n = number of samples in the sample set; Min = minimum; Max = maximum; SD = standard deviation.

The widest B content range was observed in BD 'Pelotas' (13.92 to 64.75 mg kg^{-1}, SD 7.95 mg kg^{-1}) and the smallest range was recorded for BD 'PB' (15.60 to 36.92 mg kg^{-1}, SD 5.47 mg kg^{-1}) (Figure 3a). The widest Cu content range was observed in BD 'PB' (0.84 to 27.84 mg kg^{-1}, SD 4.55 mg kg^{-1}) and the smallest range was recorded for BD 'Pelotas' (2.20 to 12.48 mg kg^{-1}, SD 1.65 mg kg^{-1}) (Figure 3b).

The content of nutrients Fe and Zn showed a wide range of values in BD 'PB' and 'Pelotas'; and the widest range was recorded for BD 'PB' (13.32 to 171.16 mg kg^{-1}, SD 19.45 mg kg^{-1} and 14.64 to 161.44 mg kg^{-1}, SD 34.50 mg kg^{-1}, respectively); the smallest range was observed for BD 'Pelotas' (24.00 to 134.70 mg kg^{-1}, SD 18.42 mg kg^{-1} and 6.60 to 85.70 mg kg^{-1}, SD 9.96 mg kg^{-1}, respectively) (Figure 3c,e).

Mn content presented the widest amplitude in comparison to the other micronutrients (B, Cu, Fe and Zn) (Figure 3a–e). The widest Mn content amplitude was observed in BD 'PB' (45.44 to 607.52 mg kg^{-1}, SD 132.82 mg kg^{-1}) and the smallest one was recorded for BD 'Pelotas' (21.98 to 406.30 mg kg^{-1}, SD 94.69 mg kg^{-1}) (Figure 3d).

3.2. Principal Component Analysis (PCA)

Based on the principal component analysis (PCA), only the first two components were taken into consideration; together, they explained 82.9% original data variance (Figure S2). Principal component 1 (PC1) explained 64.6% variability, and this finding was mainly influenced by Mn, Fe, Zn, and B contents in the leaves collected in the study sites—it showed the greatest contributions from Mn, Fe, and Zn (Figure S2). Principal component 2 (PC2) explained 18.3% data variability, and it was mainly influenced by Zn, Fe, Mn, Ca, and B contents in leaf tissue from plants collected in the study sites—it shows the greatest contribution from Zn and Fe (Figure S2).

The projected sample scores on principal components PC1 and PC2 indicated that the cultivation site is associated with the main latent gradients of variation in the dataset, as these components, defined as orthogonal linear combinations of the original variables, account for the largest proportion of the total variance, resulting in the separation of samples into two distinct groups in the multivariate space. (Figure S2). The group to the right of CP1 was formed by observations from cultivation location 2 (Pelotas), and the group to the left of the CP1 axis comprised observations from cultivation location 1 (Pinto Bandeira).

3.3. Performance and Importance of Bands in the Calibration of Prediction Models

The highest accuracies ($R^2 \geq 0.75$), i.e., models, according to which, nutrient contents estimated for peach leaves were closest to the contents found through the reference method (wet chemical analysis) resulted from the following "nutrient + model" combinations: P 'PB', K 'PB', Ca 'PB' and 'PB + Pel', Mg 'PB' and 'Pel', B 'PB' and 'PB + Pel', Cu 'PB', Mn 'Pel', Zn 'Pel' and 'PB + Pel' (Table 1). Models showing average accuracies (R2 ≥ 0.50 and < 0.75) were N 'PB' and 'Pel' and 'PB + Pel', P 'Pel' and 'PB + Pel', K 'PB + Pel', Mg 'PB + Pel', S 'PB', B 'Pel', Cu 'Pel', Fe 'PB', Mn 'PB' and 'PB + Pel' and Zn 'PB' (Table 1). The other models, K 'Pel', Ca 'Pel', Cu 'PB + Pel' and Fe 'Pel' and 'PB + Pel', recorded low accuracies ($R^2 < 0.50$); therefore, they are not recommended models (Table 1).

The metric parameter (RPIQ) used to rank the models based on their ability to estimate nutrient contents in peach leaves allowed observing that results were similar to those recorded in R^2. The models set for nutrients P 'PB', K 'PB', Ca 'PB', Mg 'PB', B 'PB' and Mn 'Pel' were included in category A (RPIQ ≥ 3.0). Category B (1.9 ≥ RPIQ < 3.0) included models N 'PB' and 'Pel' and 'PB + Pel', P 'PB + Pel', Ca 'PB + Pel', Mg 'Pel' and 'PB + Pel',

S 'PB', B 'Pel' and 'PB + Pel', Cu 'Pel', Mn 'PB' and 'PB + Pel' and Zn 'PB' and 'Pel' and 'PB + Pel', whereas category C (≥1.5 RPIQ < 1.9) comprised models P 'Pel', K 'Pel', 'PB + Pel', Ca 'Pel', Fe 'Pel' and 'PB + Pel' (Table 1). The ability to estimate these nutrient contents was even lower than the lowest limit of category C (RPIQ < 1.5) in models Cu 'PB' and 'PB + Pel' and Fe 'PB' (Table 1).

Table 1. Accuracy statistics of models calibrated at local scale, 'Pinto Bandeira—PB' and 'Pelotas—Pel' and regional 'PB + Pel' for macronutrients N, P, Ca, Mg and S, and micronutrients B, Cu, Fe, Mn and Zn.

Nutrient	Models	Nc	ncomp.	R^2c	RMSEc	MAEc	RPIQc
N	PB *	102	4	0.70	1.68	1.55	2.87
N	Pel *	273	10	0.63	3.08	2.42	2.28
N	PB + Pel	376	14	0.66	2.78	2.21	2.35
P	PB	102	10	0.82	0.09	0.07	3.07
P	Pel	273	12	0.52	0.28	0.22	1.81
P	PB + Pel	376	12	0.70	0.31	0.24	2.30
K	PB	102	28	0.97	0.55	0.33	8.08
K	Pel	273	4	0.39	2.75	2.13	1.65
K	PB + Pel	376	16	0.57	2.40	1.89	1.78
Ca	PB	102	19	0.98	0.71	0.53	8.30
Ca	Pel	273	5	0.46	2.83	2.19	1.89
Ca	PB + Pel	376	16	0.83	2.27	1.79	2.90
Mg	PB	102	17	0.96	0.17	0.10	7.86
Mg	Pel	273	12	0.76	0.83	0.67	2.96
Mg	PB + Pel	376	14	0.71	0.88	0.67	2.59
S	PB	102	5	0.70	0.23	0.18	2.09
B	PB	102	11	0.97	1.05	0.84	10.19
B	Pel	273	13	0.74	4.04	3.10	2.95
B	PB + Pel	376	16	0.80	3.85	2.86	2.94
Cu	PB	102	14	0.86	1.82	1.00	1.32
Cu	Pel	273	12	0.64	0.99	0.77	2.21
Cu	PB + Pel	376	3	0.14	2.22	1.41	1.00
Fe	PB	102	4	0.73	9.84	8.85	1.48
Fe	Pel	273	13	0.48	13.48	9.76	1.78
Fe	PB + Pel	376	9	0.42	15.20	10.93	1.57
Mn	PB	102	15	0.61	45.17	41.74	2.66
Mn	Pel	273	17	0.87	34.85	26.80	4.05
Mn	PB + Pel	376	11	0.67	62.32	45.43	2.72
Zn	PB	102	4	0.70	16.65	14.54	2.20
Zn	Pel	273	2	0.77	5.56	5.01	1.95
Zn	PB + Pel	376	3	0.90	6.89	7.54	2.87

* PB = Pinto Bandeira; * Pel = Pelotas. Nc = number of samples in the calibration step; ncomp = number of principal components used by the PLSR method; R^2c = coefficient of determination in the calibration step; RMSEc = root mean square prediction error in the calibration step; MAEc = mean absolute error in the calibration step and RPIQc = ratio of performance to interquartile in the calibration step.

The highest calibration prediction accuracy for nutrient content in peach leaf samples from two producing municipalities was recorded for P, in the 'PB' model (RMSE = 0.09 g kg^{-1}, MAE = 0.07 g kg^{-1}) in comparison to models set for the other nutrients, if one takes into account parameters RMSE and MAE. The lowest calibration prediction accuracy for

nutrient content was recorded for Mn in the 'PB + Pel' model (RMSE = 62.32 mg kg^{-1}, MAE = 45.43 mg kg^{-1}) (Table 1).

The spectral regions with relative importance greater than 75% for nutrient prediction are presented in Table 2. Overall, all nutrients exhibited their highest importance in the visible region (430–460, 550, and 660–680 nm), the red-edge region (705, 720, and 740 nm), the near-infrared (NIR; 750–1300 nm), and the shortwave infrared (SWIR; 1300–2500 nm). Models calibrated for N, P, Ca, Mg, B, and Cu at local-1 'PB' showed consistently higher importance across all these spectral regions, with a larger number of influential bands compared with the other modeling scenarios.

Table 2. Vis–NIR spectral bands showing relative importance above 75% in the prediction of each nutrient under different model scenarios.

Nutrient	Models	Vis-NIR Spectral Bands with Relative Importance > 75%
N	PB + Pel	433, 458, 460, 670, 678, 710, 711, 735, 2425, 2126, 2132, 2180, 2234, 2235, 2273, 2274, 2375, 2378
	PB *	425, 430, 461, 550, 693, 694, 695, 696, 697, 705, 710, 711, 718, 740, 1550, 1875, 1876, 1877, 1874, 1878, 2250, 2280, 2300
	Pel *	480, 680, 682, 684, 685, 683, 686, 687, 1875, 1876, 1877, 878, 2250 2426, 2434, 2471
P	PB + Pel	435, 690, 700, 710, 736, 740, 850, 852 2115, 2245, 2474, 2473, 2475, 2472 2476, 2471
	PB	430, 450, 475, 688, 735, 738, 740, 742, 800, 2100, 2226, 2467, 2467, 2468, 2469, 2470, 2470, 2493, 2495
	Pel	408, 432, 460, 563, 661, 695, 700, 810, 2111, 2225, 2289, 2310, 2426, 2467, 2473, 2480, 2474
K	PB + Pel	435, 660, 665, 705, 706, 707, 708, 709, 710, 711, 712, 713, 714, 720, 735, 740, 800, 900, 980, 1250, 1300, 2180, 2250
	PB	420, 660, 682, 684, 685, 686, 707, 708, 709, 710, 712, 717, 720, 882, 915, 1005, 1025, 1080, 1100, 1255, 2175, 2195, 2296
	Pel	438, 712, 713, 714, 740, 741, 739, 686, 682, 850, 1110, 1194, 2171, 2295
Ca	PB + Pel	425, 699, 700, 741, 739, 788, 800, 802, 810, 820, 880, 1085, 1100, 1935, 1947, 1964, 1674, 2028, 2029, 2274
	PB	698, 700, 707, 710, 800, 425, 826, 827, 910, 912, 1100, 1111, 1990, 1946, 1965, 1989, 1999, 2030, 2031, 2175, 2272, 2480
	Pel	430, 431, 480, 684, 685, 687, 697, 699, 705, 706, 711, 714, 718, 810, 912, 1008, 1100, 2174, 2175, 2272, 2274
Mg	PB + Pel	405, 464, 478, 470, 663, 664, 700, 705, 709, 710, 715, 716, 800, 910, 1005, 1110, 2021, 2022, 2193, 2194, 2292, 2350, 2285
	PB	405, 420, 450, 460, 475, 662, 664, 667, 668, 670, 671, 669, 672, 700, 702, 703, 710, 711, 715, 716, 721, 2438, 2398, 1884, 1886, 2019, 2020, 2238, 2398
	Pel	400, 405, 662, 682, 685, 687, 688, 704, 705, 714, 705, 713, 719, 722, 1885, 1888, 1890, 2019, 2020, 2185, 2194, 2220
S	PB	405, 685, 687, 705, 714, 718, 720, 735, 740, 741, 1439, 1450, 1511, 1550, 1556, 1560, 1880, 1935, 1940, 2058, 2182, 2266, 2281
B	PB + Pel	424, 538, 539, 541, 544, 545, 641, 642, 644, 646, 648, 692, 694, 696, 698, 699, 1335, 1450, 1565, 1940, 2100, 2287, 2289, 2290, 2291, 2292, 2294, 2287, 2300
	PB	407, 693, 696, 697, 718, 717, 719, 720, 1455, 1550, 1551, 1878, 1874, 1876, 1880, 1882, 1885, 1887, 1891, 1893, 1895, 1897, 1898, 1900, 1925, 1940, 2000, 2100, 2225, 2300
	Pel	421, 422, 645, 664, 690, 692, 693, 694, 696, 716, 717, 721, 1335, 1400, 1450, 1550, 1883, 1874, 1884, 1998, 2100, 2317, 2318, 2319, 2316, 2330,
Cu	PB + Pel	710, 714, 715, 800, 850, 968, 969, 967, 1460, 1520, 1560, 1910, 1940, 1801, 1878, 1900, 1940, 2225, 2298, 2451, 2470
	PB	400, 643, 644, 686, 687, 691, 692, 693, 694, 691, 703, 707, 710, 714, 716, 719, 968, 969, 970, 800, 889, 1435, 1460, 1510, 1520, 1525, 1800, 1801, 2414, 2449, 2450, 2495, 2414, 2487
	Pel	707, 710, 714, 716, 719, 968, 969, 967, 970, 800, 889, 1435, 1460, 1510, 1520, 1525, 1560, 1910, 1940, 1801, 1877, 1878, 1900, 1940, 2110, 2222
Fe	PB + Pel	635, 650, 705, 720, 725, 740, 750 751, 753, 754, 756, 758, 1351, 1352, 1355, 1363, 1389, 1435, 1875, 1877, 1878, 1879, 2247, 2258, 2332
	PB	540, 635, 640, 650, 705, 720, 725, 740, 750 751, 753, 754, 756, 758, 1351, 1352, 1355, 1363, 1389, 1435, 1875, 1876, 1877, 1878, 1879, 2247, 2258, 2332, 2444,2450
	Pel	410, 354, 366, 361, 673, 674, 672, 675, 671, 676, 670, 677, 669, 1897, 1899, 1894, 668, 678, 1893, 1901, 2246, 1892, 2247, 2248
Mn	PB + Pel	422, 635, 644, 645, 687, 686, 689, 646, 748, 756, 685, 689, 646, 731, 747, 749, 750, 752, 753, 754, 755, 1892, 2247, 2248, 1903, 2245, 2249, 2244, 667, 2250

	PB	425, 644, 635, 704, 720, 721, 738, 752, 357, 645, 753, 750, 1891, 1889, 1895, 1887, 1880, 1878, 1881, 1885, 1898, 1876, 1899, 2245, 2249, 2250
	Pel	430, 682, 678, 679, 680, 686, 689, 692, 693, 705, 706, 709, 710, 712, 715, 717, 720, 721, 740, 1887, 1880, 1878, 1881, 1885, 2245, 2249, 2246, 2255
Zn	PB + Pel	685, 686, 705, 720, 740, 744, 747, 748, 1392, 1399, 1400, 1403, 1404, 1405, 1450, 1510, 1560, 1875, 1898, 1940, 2100, 2300
	PB	423, 480, 656, 679, 678, 680, 681 685, 660, 677, 682, 694, 695, 1405, 1450, 1510, 1560, 1667, 1870, 1940, 2285
	Pel	410, 683, 686, 687, 690, 692, 693, 1375, 1400, 1405, 1450, 1510, 1560, 1885, 1889, 1891, 1892,1875, 1940, 2228

* PB = Pinto Bandeira; * Pel = Pelotas.

3.4. Validation of Prediction Models

The highest accuracies take into account parameter R^2 ($R^2 \geq 0.75$) in model validations; in other words, the estimated content closest to those found through the reference method (wet chemistry) resulted from the following "macronutrients + model" combinations: P 'PB', Ca 'PB' and 'PB + Pelotas', Mg 'PB' (Figures 4b and 5a,b). Models with medium accuracies ($R^2 \geq 0.50$ and < 0.75) were N 'PB', P 'PB + Pelotas', K 'PB', Mg 'Pelotas' and 'PB + Pelotas', S 'PB' (Figures 4a–c and 5b,c). With respect to the other models, the ability of N 'Pelotas' and 'PB + Pelotas', P 'Pelotas', K 'Pelotas' and 'PB + Pelotas', Ca 'Pelotas' to estimate these nutrients' content was low ($R^2 < 0.50$); therefore, these models are not recommended (Figures 4a–c and 5a).

The use of other metric RPIQ parameters to assess the models' ability to estimate macronutrient contents in peach leaves showed results similar to those observed for R^2. Models set for macronutrients Ca (PB) and 'PB + Pel' and Mg (PB) were included in category A (RPIQ ≥ 3.0) (Figures 4a, b). Category B (1.9 ≥ RPIQ < 3.0) included models N 'Pelotas', P 'PB' and 'PB + Pelotas', K 'PB', Mg 'Pelotas' and 'PB + Pelotas' (Figures 4a–c and 5b), whereas category C (≥1.5 RPIQ < 1.9) comprised models N 'PB + Pelotas', P 'Pelotas', K 'PB + Pelotas', Ca 'Pelotas' and S 'PB' (Figures 4a–c and 5a,c). The capacity of models N 'PB' and K 'Pelotas' to estimate these nutrients' contents was even lower than the lowest limit set for category C (RPIQ < 1.5) (Figure 4a,c).

The highest validation prediction accuracy of macronutrient contents in peach leaf samples was observed for P in the 'PB' model (RMSE = 0.10 g kg^{-1}, MAE = 0.14 g kg^{-1}) in comparison to models set for the other macronutrients if one takes into consideration parameters RMSE and MAE (Figure 4b). The lowest accuracy recorded for validation predictions of macronutrient contents was observed for N in the 'Pelotas' model (RMSE = 3.62 g kg^{-1}, MAE = 2.85 g kg^{-1}) (Figure 4a).

The highest accuracies were recorded by taking into account parameter R^2 ($R^2 \geq 0.75$), which means, estimated contents closest to those found through the reference method (wet chemical analysis) were the "micronutrients + model" combinations B 'PB' and 'PB + Pelotas', Cu 'PB' and Zn 'PB + Pelotas' (Figure 6a,b,e). Models accounting for medium accuracies ($R^2 \geq 0.50$ and < 0.75) were B 'Pelotas', Fe 'PB', Mn 'PB' and 'Pelotas' and 'PB + Pelotas', Zn 'PB' and 'Pelotas' (Figure 6a,c,d,e). In addition, the ability of Cu 'Pelotas' and 'PB + Pelotas', Fe 'Pelotas' and 'PB + Pelotas' models to estimate these nutrients' contents was low ($R^2 < 0.50$); therefore, they are not recommended models (Figure 6b,c).

It was observed that the results, when the metric parameter (RPIQ) was used to assess the models' ability to estimate the content of micronutrients found in peach leaves, are different from those found through R^2. Only the model set for micronutrient B 'PB' was included in category A (RPIQ ≥ 3.0) (Figure 6a). Category B (1.9 ≥ RPIQ < 3.0) included models B 'PB + Pelotas', Cu 'Pelotas', Mn 'PB' and 'Pelotas', Zn 'PB' and 'PB + Pelotas' (Figure 6a,b,d,e), whereas category C (≥1.5 RPIQ < 1.9) comprised models B 'Pelotas' and Fe 'Pelotas' (Figure 6a,c). The capacity of models Cu 'PB' and 'PB + Pelotas', Fe 'PB' and 'PB + Pelotas', Zn 'Pelotas' to estimate these nutrients' content was even lower than the lowest limit set for category C (RPIQ < 1.5) (Figure 6b,c,e).

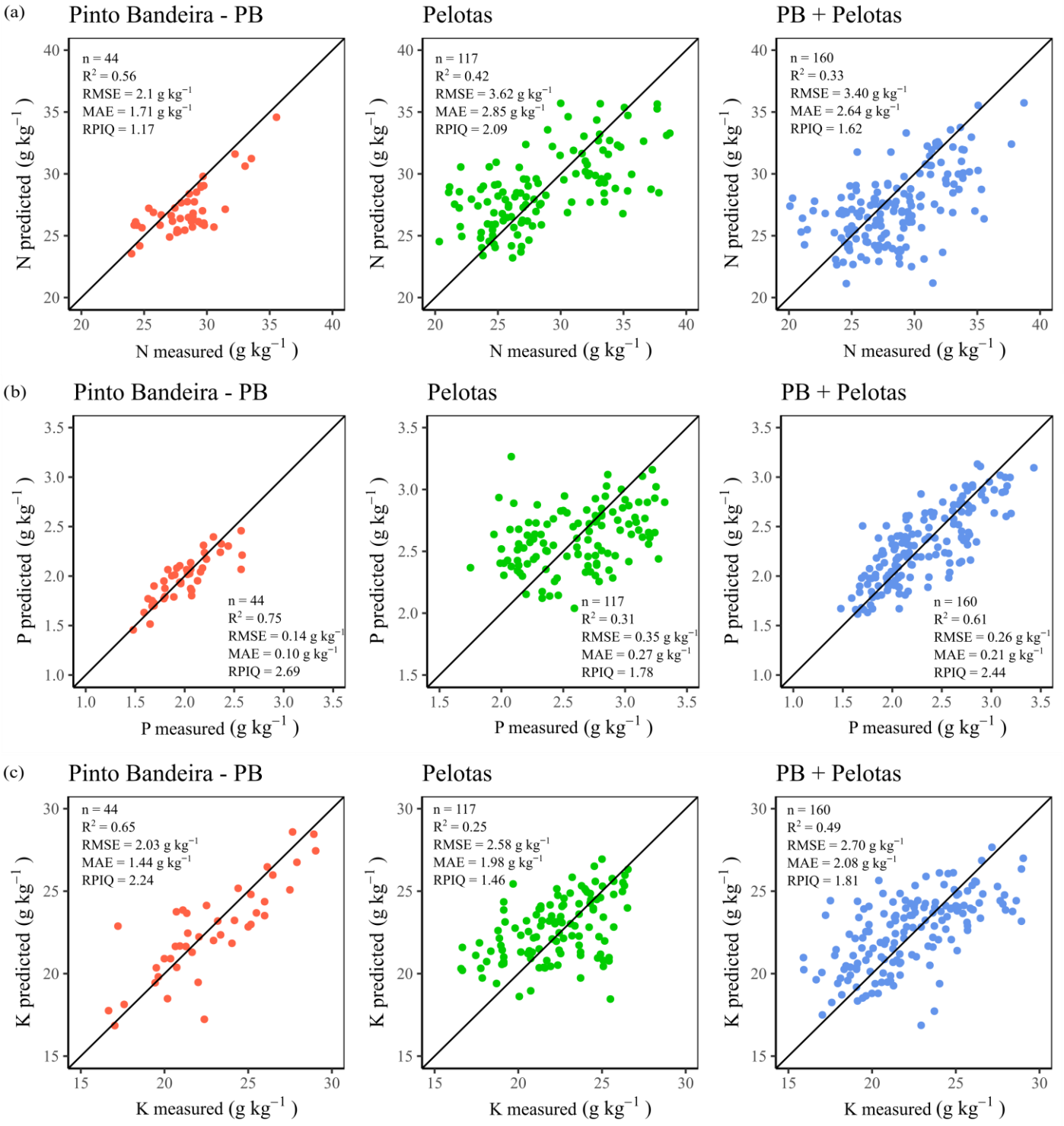

Figure 4. Association between measured contents (wet chemistry method) and predicted contents through the three models: 'PB', 'Pelotas' and 'PB + Pelotas' set for macronutrients N (**a**), P (**b**) and K (**c**). PB = *Pinto Bandeira*; n = number of samples; R^2 = coefficient of determination; RMSE = root mean square prediction error; MAE = mean absolute error and RPIQ = ratio of performance to interquartile.

https://doi.org/10.3390/horticulturae12030296

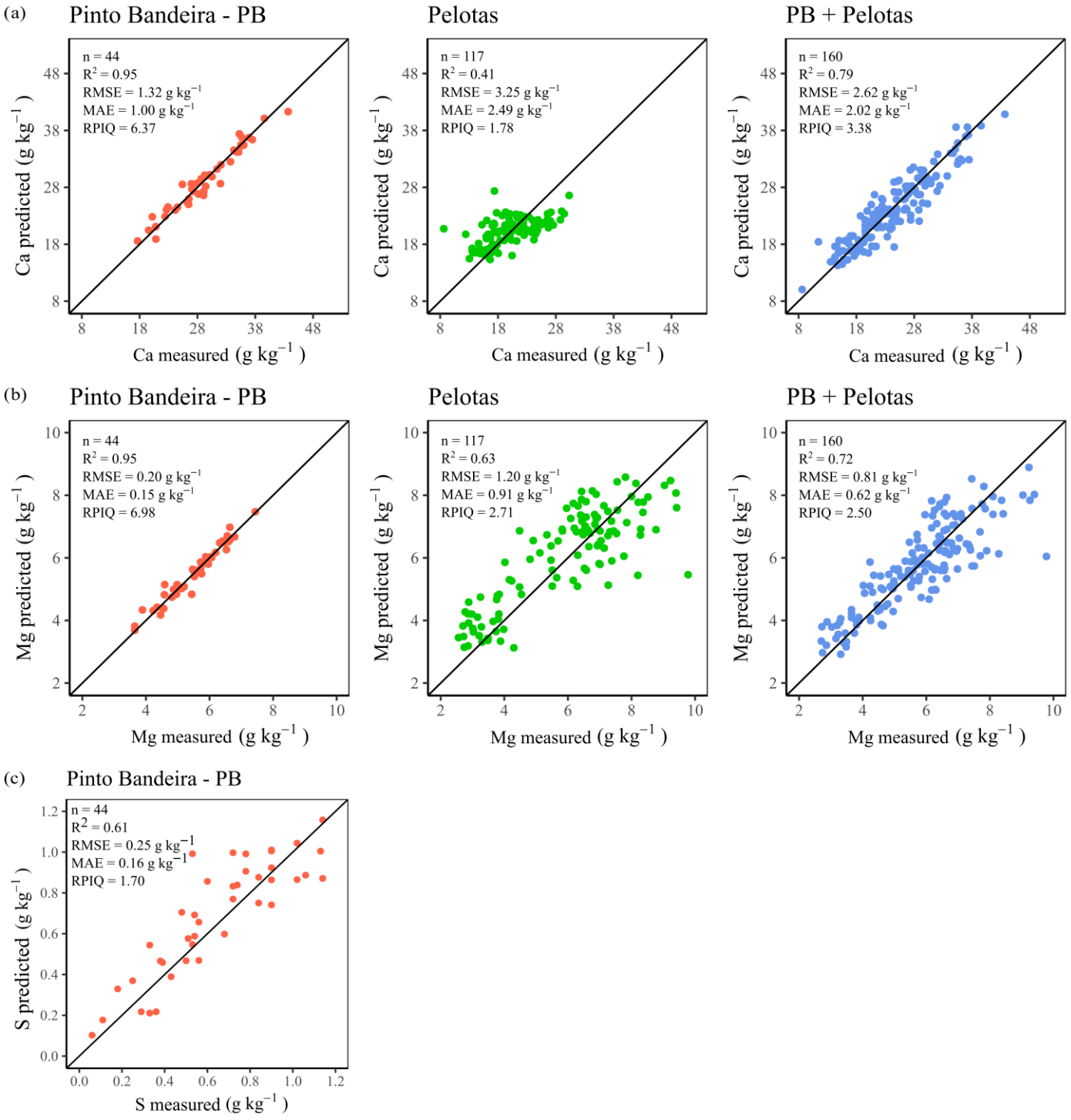

Figure 5. Association between measured contents (wet chemistry method) and predicted contents through the three models 'PB', 'Pelotas' and 'PB + Pelotas' set for macronutrients Ca (**a**), Mg (**b**) and S (**c**). PB = *Pinto Bandeira*; n = number of samples; R^2 = coefficient of determination; RMSE = root mean square prediction error; MAE = mean absolute error and RPIQ = ratio of performance to interquartile.

The highest accuracy in predicting micronutrient contents in peach leaf samples collected from two producing municipalities was recorded for Cu in the 'Pelotas' model (RMSE = 1.30 mg kg^{-1}, MAE = 1.04 mg kg^{-1}) in comparison to models set for the other micronutrients, if one takes into account parameters RMSE and MAE (Figure 6b). The

lowest accuracy in predicting micronutrient contents was observed for Mn in the 'PB + Pelotas' model (RMSE = 76.92 mg kg^{-1}, MAE = 58.26 g kg^{-1}) (Figure 6d).

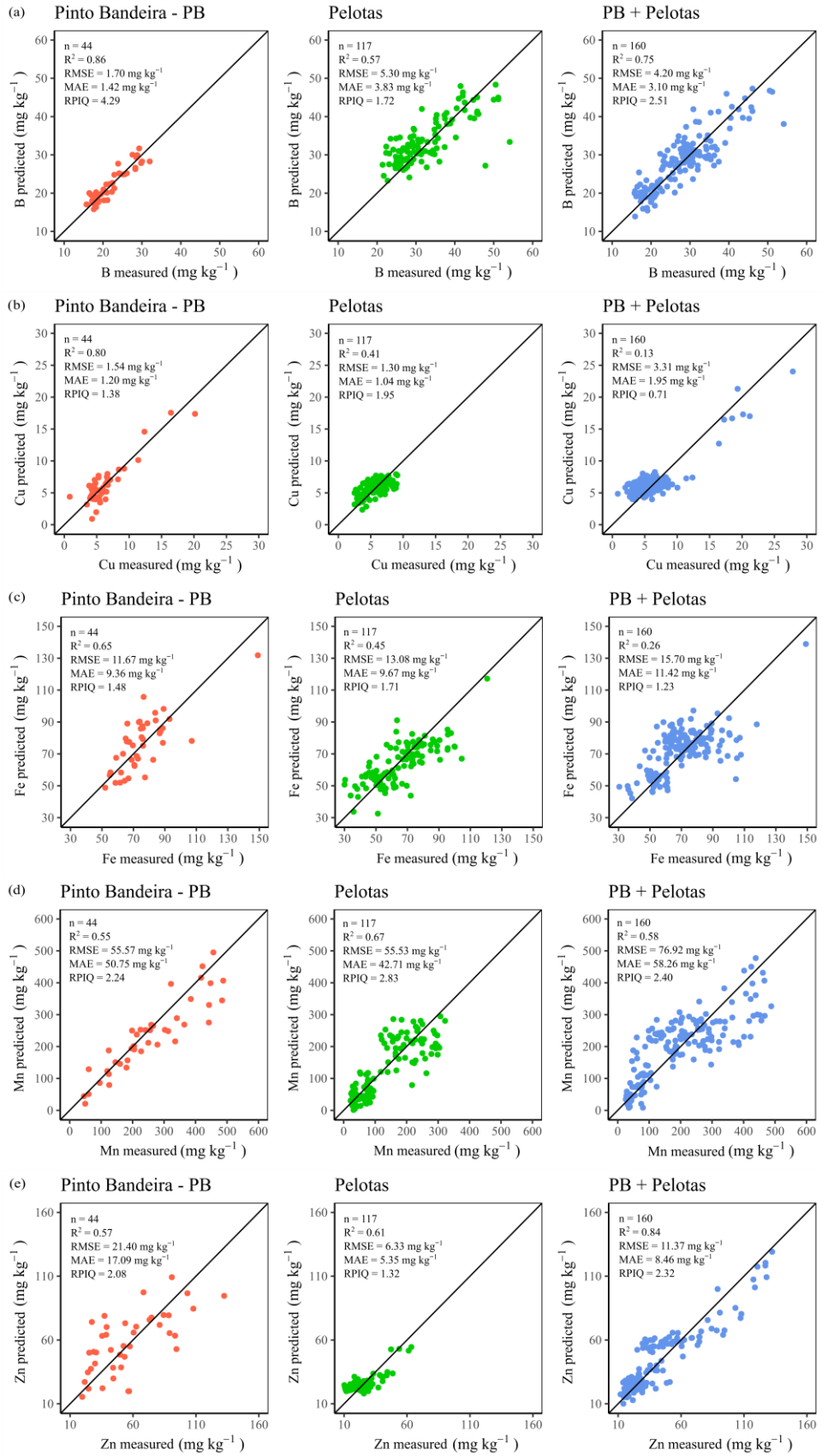

Figure 6. Association between measured contents (wet chemistry method) and predicted contents found through the three models: 'PB', 'Pelotas' and 'PB + Pelotas' set for micronutrients B (**a**), Cu

(**b**), Fe (**c**), Mn (**d**) and Zn (**e**). PB = *Pinto Bandeira*; n = number of samples; R^2 = coefficient of determination; RMSE = root mean square prediction error; MAE = mean absolute error and RPIQ = ratio of performance to interquartile.

3.5. Prediction Models Application to Different Databases

The three prediction models (regional, local-1, local-2) were applied to different databases in order to simulate their applicability across the data coverage scale at this stage. local-1 model 'PB' performed satisfactorily for macronutrients N, P, K, Ca, and Mg since it presented lower MAE values than the regional model (PB + Pel) (Figure 7a–e).

On the other hand, model local-2 'Pelotas' recorded higher MAE values than the regional model 'PB + Pel' set for N, P, Ca and Mg (Figure 7a,b,d,e). Model local-2 'Pelotas' only presented satisfactory performance for K since it recorded a lower MAE value than the regional model 'PB + Pel' (Figure 7c). Furthermore, there was a significant increase in MAE value whenever the model calibrated for local-1 'PB' was applied to data from local-2 'Pelotas'; the same was observed when the model calibrated for local-2 'Pelotas' was applied to data from local-1 'PB' (Figure 7a–e). MAE values set for macronutrients K and Ca were very close to those observed for data from 'PB + Pel' when the regional model 'PB + Pel' was applied to data from local-1 'PB' and local-2 'Pelotas' (Figure 7c,d).

Model local-1 'PB' recorded satisfactory performance for micronutrients B, Cu, Fe, and Mn since it presented lower MAE values than the regional 'PB + Pel' model (Figure 8a–d). Model local-1 'PB' model only presented higher MAE values than the regional 'PB + Pel' model set for the micronutrient Zn (Figure 8e).

Model local-2 'Pelotas' presented satisfactory performance for micronutrients Cu, Fe, Mn, and Zn because it presented lower MAE values than the regional model 'PB + Pel' (Figure 8b–e). Model local-2 'Pelotas' only recorded a higher MAE value than the regional model 'PB + Pel' for micronutrient B (Figure 8a). In addition, there was a significant increase in the MAE value when the model calibrated for local-1 'PB' was applied to data from local-2 'Pelotas'. The same happened when the model calibrated for local-2 'Pelotas' was applied to data from local-1 'PB' (Figure 8a–e). Furthermore, when it comes to micronutrients B, Cu, Fe and Mn, it was possible to observe that MAE values were similar to those recorded when the regional model was applied to the regional database, when the regional model 'PB + Pel' was adopted to data from locations 'PB' and 'Pelotas', separately (Figure 7a–d).

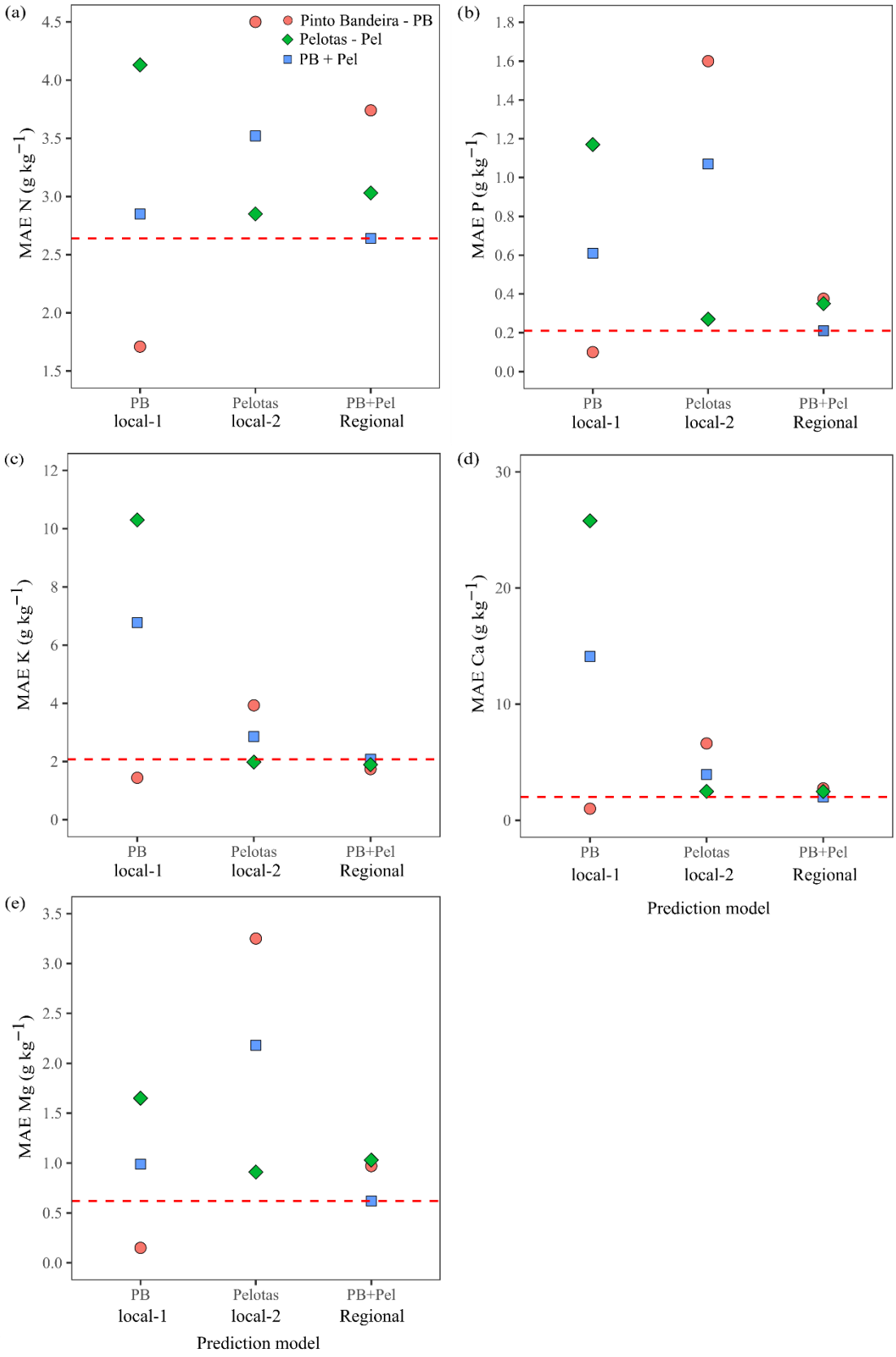

Figure 7. Assessing the performance of the three prediction models: Model 2—'PB', Model 3—'Pelotas', Model 1—'PB + Pel' set for macronutrients (N (**a**), P (**b**), K (**c**), Ca (**d**) and Mg (**e**)) in leaves by applying the mean absolute error (MAE). PB = Pinto Bandeira; Pel = Pelotas. The red dashed line represents the MAE value in regional model 'PB + Pel' validation.

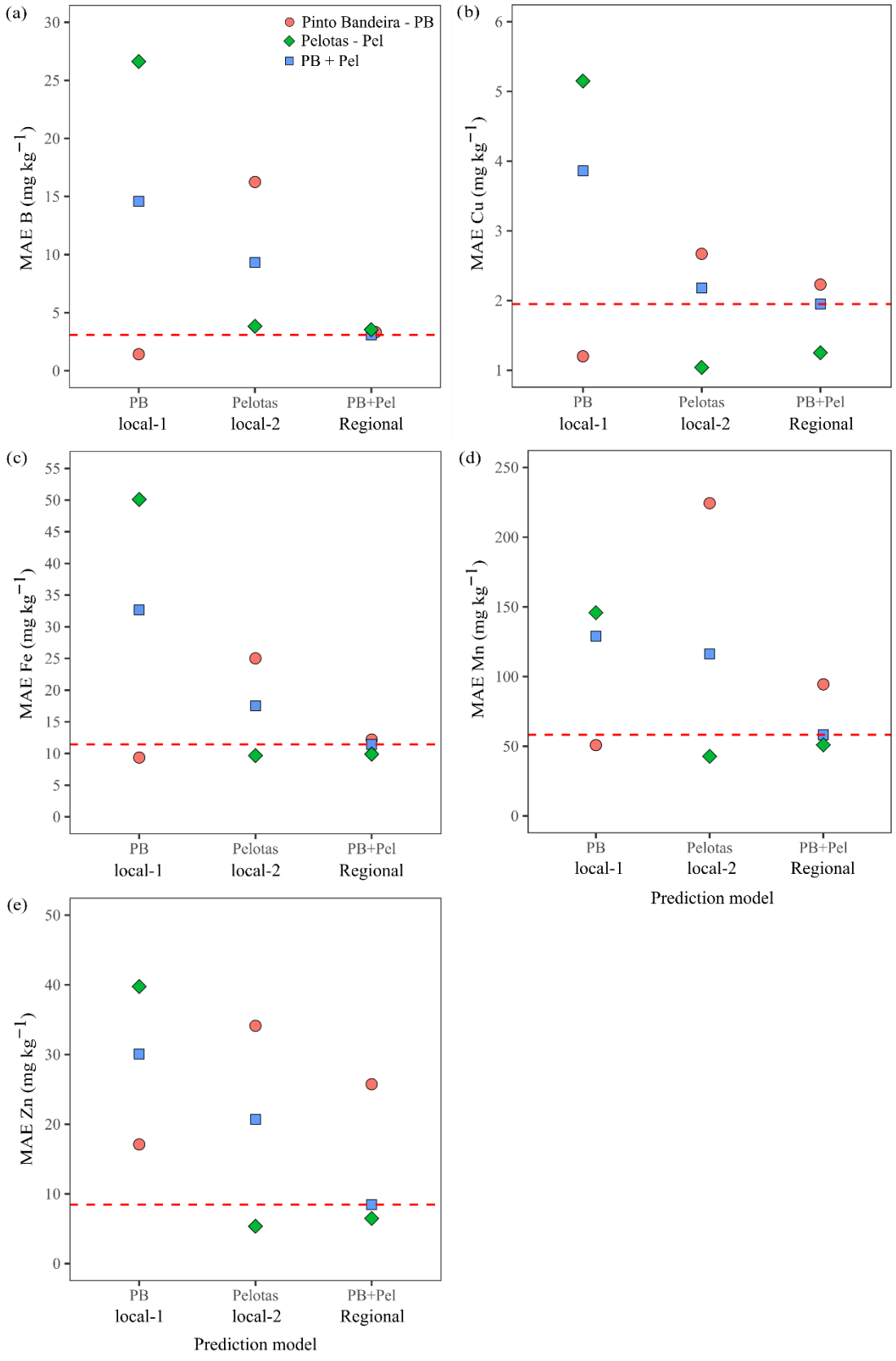

Figure 8. Assessing the performance of the three prediction models: Model 2—'PB', Model 3—'Pelotas', Model 1—'PB + Pel' set for micronutrients B (**a**), Cu (**b**), Fe (**c**), Mn (**d**) and Zn (**e**) in leaves by using mean absolute error (MAE). PB = Pinto Bandeira; Pel = Pelotas. The red dashed line represents the MAE value in regional model 'PB + Pel' validation.

https://doi.org/10.3390/horticulturae12030296

The accuracy to classify nutrient estimates based on SR (Table S2) in comparison to values found through the reference method is shown in Figure 9. The three models presented low accuracy percentage (<80%) for N; however, model local-1 'PB' presented a value close to 80%. The regional models 'PB + Pelotas' and local-1 'PB' presented a high accuracy percentage (≥90%) for nutrients P, Ca, and B, whereas model local-2 'Pelotas' recorded a low accuracy percentage (66%). Regional and local-1 'PB' models showed low accuracy percentage (<70%) for K, and model local-2 'Pelotas' presented a high accuracy percentage (88%). The three models showed a high accuracy percentage (≥90%) for Mg, with emphasis on estimates of model local-1 'PB', which recoded 100% accuracy. Model local-1 'PB' presented a low accuracy percentage (<70%) for nutrients S and Fe. Regional model 'PB + Pelotas' and local-2 'Pelotas' showed a high accuracy percentage (≥ 85%) for Fe. Model local-1 'PB' recorded a high accuracy percentage (86%) for Cu, whereas the regional model 'PB + Pelotas' and model local-2 'Pelotas' recorded low accuracy percentage for them (<55%) (Figure 9).

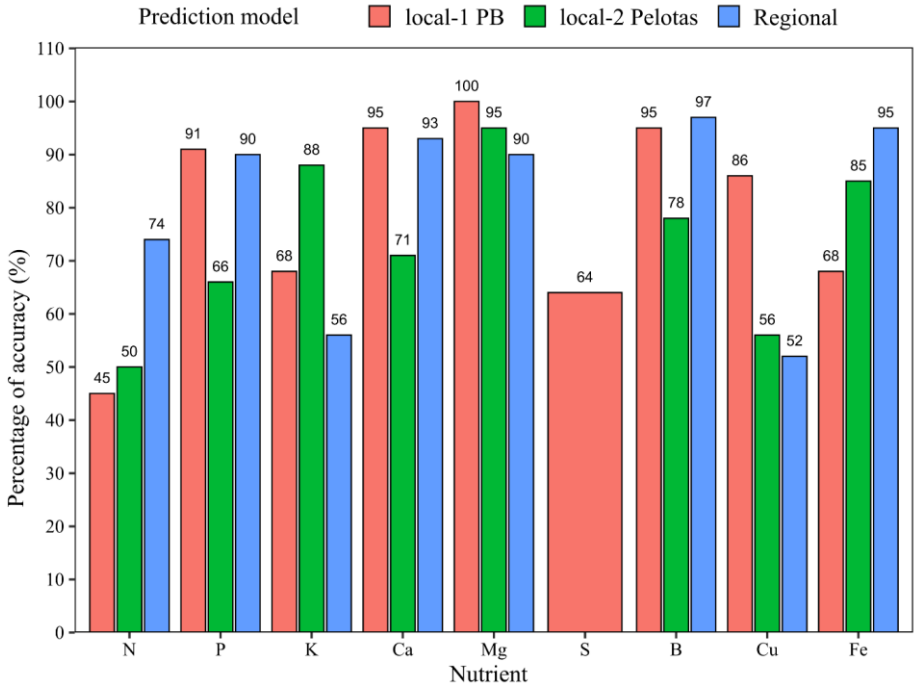

Figure 9. Classification accuracy (%) of nutrient concentrations predicted by Vis–NIR models into adequacy classes—within the sufficiency range (SR) and above the SR—according to the proposed sufficiency ranges for Southern Brazil (Table S2) [37].

4. Discussion

The contents of the 11 herein assessed nutrients recorded a wide range of values (Figures 2 and 3). This is a desirable feature because the presence of such a wide range of values in a spectral library is essential for the generation of robust models [14] since they have larger prediction intervals. However, some nutrients (N, K, Ca, B, Cu, Zn, and Mn) presented high standard deviations for these values in some LSL, notably local-1 'Pel' and regional 'PB + Pel'. This is a negative feature for a spectral library, since it can reduce the accuracy of prediction models based on spectral data [14,38]. Additionally, regarding S data, the low amplitude of values observed in the local-1 'PB' database, together with the absence of this element in the local-2 'Pel' database, represents a clear limitation for the development and interpretation of models generated for S.

The amplitude and variance of nutrient contents in peach leaves from the three LSL (regional, local-1, and local-2) were different (Figures 2 and 3). The highest variance was

observed for Ca contents in regional LSL 'PB + Pel' (SD 5.55 g kg^{-1}), and for N in both local-2 LSL 'Pel' (SD 5.00 g kg^{-1}) and regional 'PB + Pel' (SD 4.51 g kg^{-1}) among the assessed macronutrients (Figure 2d and a, respectively). This feature can be explained by the fact that leaf samples came from different orchards, namely, commercial orchards in Pinto Bandeira and experimental orchards in Pelotas. Commercial orchards often face frequent applications of Ca-based products on the leaves throughout the crop's production cycle to provide Ca and achieve adequate fruit development—it is of great importance for several cell wall structures, besides influencing fruit conservation [39]. 'PB' and 'Pelotas' soils are different; consequently, they present broad variations in organic matter contents. Orchards in 'Pelotas' orchards have lower organic matter contents (Table S1); consequently, there is less availability of mineral forms of native N to plants [40]. Furthermore, peach productivity was higher in 'PB' than in 'Pelotas', for example, and it increased the demand for N, because the amounts of N exported by the fruits are larger [41,42]. Therefore, there is high variation in N contents in the orchards. In addition, the orchards' leaf samples collected in 'Pelotas' came from experiments subjected to different N doses.

Overall, the highest variations were mainly observed in the contents of micronutrients Fe, Mn, and Zn in LSL local-1 'PB' (Figure 3c–e). These wider amplitudes can be attributed to the long history of successive Cu- and Mn-based leaf fungicides applications to control fungal diseases [43,44], as well as to physicochemical features such as the amount and type of clay minerals, Fe and Mn oxides and hydroxides in the soils of the assessed municipalities [45]. Variations in these features lead to the widest amplitudes of Fe, Mn, and Zn values and, consequently, to higher variance (Figure 3c–e).

P contents in LSL local-1 'PB' showed little variation, which was represented by the lowest SD (P = 0.23 g kg^{-1}) (Figure 2b). The low variation in P content in leaves, which is among the lowest in macronutrients, may have resulted from P's high mobility in plant tissue or from the low response of fruit species (adults), such as peach trees, to phosphorus fertilization [41]. In addition, soils in the orchards where leaf samples were collected from recorded high P contents (Table S1), even higher than those set for classes established as very high by the regional fertilization manual for Rio Grande do Sul and Santa Catarina states [19]. On the other hand, orchards where leaf samples were collected from receive frequent applications of high N rates, and this can reduce leaf P contents [46] and protein synthesis due to low P availability [47].

The combination of spectral data to PLSR multivariate technique enabled calibrating prediction models with good accuracy for most nutrients (local-1 'PB', P, K, Ca, Mg and B; local-2 'Pel', Mn) (Table 1), despite the small number (between 102 and 376) of observations used in model calibration. This finding explained the PLSR method's potential to establish correlations between 2150 spectral variables derived from the Vis-NIR band and nutrient contents. This large number of multicollinear explanatory variables makes it difficult for simpler models, such as multiple linear regression models, to establish correlations that could result in accurate models [48,49]. The 2150 spectral variables were grouped into principal components that best explain data variance in the PLSR method; therefore, correlations are established to calibrate the prediction models [48].

The concentration of spectral importance above 75% across the Vis, red-edge, NIR, and SWIR regions indicates that nutrient prediction is driven by an integrated spectral response associated with leaf pigments, internal structure, and chemical composition rather than by isolated absorption features. The visible region (430–460, 550, and 660–680 nm) reflects variations in chlorophyll absorption, which are directly or indirectly influenced by nutrient availability through effects on photosynthetic capacity and leaf senescence [50,51]. The red-edge region (705, 720, and 740 nm), known for its high sensitivity to subtle changes in chlorophyll content and overall leaf biochemical status, further reinforces the link between nutrient supply and plant physiological condition [50,51]. In the

NIR region (750–1300 nm), reflectance is primarily governed by leaf internal structure, including cell walls and intercellular spaces, which are affected by nutrients involved in cell integrity and growth processes [50,51]. The SWIR region (1300–2500 nm) captures absorption features related to fundamental chemical bonds (O–H, N–H, and C–H), providing more direct information on organic compounds associated with nutrient content [50,51]. The consistently higher number of influential bands observed in the models calibrated for site 1 (PB), particularly for N, P, Ca, Mg, B, and Cu, suggests that local conditions enhanced the expression of nutrient-related physiological and biochemical variations in the spectral signal, resulting in more informative and robust prediction models compared with the other modeling scenarios.

Some models showed limited accuracy in predicting the concentration of specific nutrients, including N and Mn in the regional database, Ca at local-2 'Pel', Zn at local-1 'PB', and Cu and Fe across all datasets. Model performance was strongly associated with the range and variability of nutrient concentrations derived from foliar analyses. In particular, N, Ca, Cu, Fe, Mn, and Zn exhibited wide concentration ranges and high standard deviations (Figures 2 and 3), which negatively affected prediction accuracy, especially in smaller datasets such as those from local-1 'PB'. High variability combined with a limited number of observations tends to increase model uncertainty and reduce predictive stability. Similar effects on the accuracy of foliar nutrient prediction models have been reported in studies with grapevine, mango and banana [10], and yerba mate [11,12].

Although variability in nutrient concentrations partially explains differences in model performance, the lower predictability observed for certain nutrients—such as N, Fe, Mn, and Zn across the datasets—can also be attributed to intrinsic spectral and physiological limitations [52,53]. Most macro- and micronutrients, including Cu, Fe, Mn, and Zn, do not exhibit direct and distinct absorption features in the Vis-NIR spectral range. Consequently, their estimation relies on indirect relationships mediated by biochemical and structural leaf constituents, such as chlorophyll, proteins, and enzyme activity. These indirect associations are often weak and unstable, particularly when nutrient availability does not impose strong physiological constraints on plant metabolism. Nitrogen represents a partial exception, given its close association with chlorophyll and proteins that exhibit clear spectral responses in the Vis region. However, when N concentrations span wide ranges or include predominantly non-limiting levels—as observed in the present dataset—the spectral response may become saturated, reducing sensitivity and compromising predictive accuracy. This limitation is further exacerbated in heterogeneous datasets that integrate multiple locations, cultivars, and management conditions, where confounding factors can mask nutrient-related spectral signals.

For micronutrients such as Cu and Fe, prediction is particularly challenging because they are required in very small quantities and primarily function as enzymatic cofactors. As a result, they induce subtle physiological changes that are not consistently expressed in leaf reflectance spectra [53]. Consequently, the spectral signal-to-noise ratio associated with these elements is low, leading to reduced model robustness across locations and datasets.

Manganese represents an intermediate case. Although it plays a key role in photosystem II and can influence chlorophyll fluorescence and leaf pigmentation, its spectral effects are often masked by other factors, including leaf structural properties, water content, and interactions with other nutrients. These confounding effects may explain the lower predictability of Mn, particularly in larger and more heterogeneous regional models [53]. Overall, these results indicate that the reduced accuracy observed for specific nutrients is not solely a consequence of model limitations, but rather reflects inherent constraints of reflectance-based spectral data, combined with the nutrient-specific physiological mechanisms governing their expression in plant tissues. This finding underscores the need for cautious interpretation of prediction models for elements with weak or indirect

spectral signatures, especially when applied to heterogeneous datasets or databases with limited sample size [10,11].

Overall, accuracy assessment at the prediction models' calibration stage showed that models local-1 'PB' (P, K, Ca, Mg, and B) and local-2 'Pel' (Mn) presented higher accuracy ($R^2 \geq 0.75$, RPIQ ≥ 3.0) than the regional model 'PB + Pel' set for most nutrients (Table 1). This finding can be related to the high standard deviation recorded based on data from the regional model 'PB + Pel' set for most nutrients (Figures 2 and 3). This outcome points out the effect of LSL standard deviation on the estimates, besides showing that the strategy of separating the database into local models has some potential within this scenario because sample sets with both a wide prediction interval and the standard deviation of target variable values can lead to higher prediction errors [54–56].

The predicted models' accuracy assessment applied to each nutrient at the validation stage allowed observing that few models presented high accuracy ($R^2 \geq 0.75$, RPIQ ≥ 3.0), namely: Ca, Mg, and B models set for local-1 'PB', and the Ca model set for regional model 'PB + Pelotas'. The high accuracy of these prediction models is related to the lower standard deviation recorded for LSL target variable values. In addition, some models that had presented high accuracy at the calibration stage (Table 1) did not hold such high accuracy at model validation. It often happens in models that present RPIQ < 3.0 at the calibration stage; it points out that the model can present low accuracy when it is subjected to an external database [35,36]. This finding corroborates what was observed in the prediction yerba [13,14]. This effect was also observed in another study that predicted nutrient K in peach leaves by using hyperspectral images and multivariate analysis. Accuracy at the calibration and validation stages differed if parameters R^2 and RMSE were taken into account [57]. Gálvez-Sola [9] sought to estimate nutrient contents in citrus leaves by using near-infrared reflectance spectroscopy and observed that the models' accuracy decreased from the calibration to the validation stage.

The analysis of models' accuracy at the validation stage showed that model local-1 'PB' recorded higher accuracy in predicting nutrients such as Ca, Mg, and B in comparison to model local-2 'Pelotas' and to regional model 'PB + Pelotas'. This outcome highlights that local models can be more accurate than regional models in scenarios where regional LSL shows high standard deviation based on target variable data. The lower accuracy presented by the model regional 'PB + Pelotas' for some nutrients results from the higher standard deviation recorded for nutrient contents.

Overall, local models perform satisfactorily when they are applied to data from the same site, such as where the model was calibrated (Figures 7 and 8). However, with respect to some nutrients, such as K, for the 'PB' model, and Fe, Mn, and Zn, for the 'Pel' model, local models can also be applied to regional data—they recorded highly accurate results (Figures 7 and 8). This finding highlights that local models can yield more accurate predictions of nutrient contents than regional models, depending on LSL calibration characteristics such as narrower prediction intervals and lower standard deviation of the target variable [54–56]. This behavior was also observed during the calibration of regional and local models for estimating soil organic carbon using Vis-NIR spectral data [38].

Although the PCA (Figure S2) revealed differences among regions, the local-1 'PB', local-2 'Pel', and regional models showed similar predictive accuracies in some cases. This behavior was observed for the macronutrients K, Ca, and Mg (Figure 7c–e) and the micronutrients B and Fe (Figure 8a,c), for which all three models achieved comparable performance. This convergence in accuracy can be explained by the similarity in the range and variability of nutrient concentrations among the datasets, as model robustness and transferability tend to increase when calibration and prediction domains share similar statistical properties, even under spectral or regional heterogeneity [14,58,59].

In this context, although initially, predictive models based on Vis–NIR spectroscopy for leaf nutrient content are expected to operate independently of location, studies have demonstrated that their performance is strongly dependent on the spatial and environmental context in which they are calibrated. The literature indicates that variations associated with the cultivation site, such as edaphoclimatic conditions, management practices, genotype, phenological stage, and plant physiological characteristics, significantly influence leaf spectral responses, thereby limiting the robustness and transferability of locally calibrated models when applied to other regions [59]. Consequently, Vis-NIR models developed using restricted spectral libraries often exhibit a marked decline in predictive accuracy outside the original sampling domain, highlighting the need for more representative spectral libraries, regional or global calibration strategies, and the adoption of spiking or transfer learning approaches to enhance model robustness across geographic space.

The low accuracy of most herein predicted models can be influenced by several factors. One of them relates to errors that can come up during nutrients' wet chemical analysis; these nutrients are used as reference at the model calibration stage [58–60]. It happens when one works with a spectral library organized based on analytical data derived from different laboratories and/or determined by different analysis methods [13,58]. This process can result in not entirely correct values combined to high standard deviation [14,55,56]. It exacerbates when the number of observations in the spectral library is small, often smaller than 500. Furthermore, the low accuracy in predicting some nutrients can be explained by their extremely low contents in leaves [13,15,60].

Regarding practical field diagnostic applicability, models with prediction accuracy exceeding 80% (Figure 9) can be considered sufficiently reliable. In this context, the prediction models developed for local-1 'PB' for nutrients P, Ca, Mg and B; set for local-2 'Pelotas' for nutrients K, Mg, and Fe; and set for regional 'PB + Pelotas' for nutrients P, K, Ca, Mg, B, and Fe can be applied to interpret the nutritional status of peach trees grown in these locations, in Southern Brazil. This result is the consequence of the high accuracy of these models' calibration and validation stages (Table 1 and Figures 4–6), as previously explained.

However, further calibration studies based on more robust and representative databases are required, incorporating a larger number of samples ($n \geq 500$), different peach cultivars, and data from multiple regions of Brazil, as well as other peach-producing regions worldwide, in order to enhance the representativeness of the LSL. In addition, the evaluation of alternative spectral domains, such as the mid-infrared (MIR) region (2500–5000 nm), should be explored, as these wavelengths may provide complementary information not captured in the VIS-NIR range. Together, these advances will support the development of standardized protocols for implementing spectroscopy combined with multivariate techniquein routine laboratory diagnostics.

5. Conclusions

Spectral data collected from local LSL '*Pinto Bandeira*' and '*Pelotas*' through the Vis-NIR spectroscopy technique in combination to the PLSR multivariate techniquemethod estimated the contents of nutrients such as Ca, Mg and B in the local 'PB' models and as Ca in the regional 'PB + Pel' model applied to peach tree leaves with high accuracy ($R^2 \geq 0.75$, $RPIQ \geq 3.0$).

The standard deviation recorded for nutrient contents in each LSL influenced the accuracy of prediction models, because LSL recording a high standard deviation led to lower accuracy estimates.

Model local-1 'PB' showed higher prediction accuracy than the local-2 model 'Pelotas' and the regional model 'PB + Pelotas'.

https://doi.org/10.3390/horticulturae12030296

Most of the herein proposed prediction models showed average accuracy ($R^2 \geq 0.50$ and <0.75, RPIQ ≥ 1.9 and <3.0); the lowest accuracies were observed for nutrients N and Mn in the regional model 'PB + Pel'.

Estimates for nutrient contents in peach tree leaves from local models, local-1 'PB' and local-2 'Pelotas' applied to data from the same site performed better than when they were applied to data from other sites and/or regions.

Finally, the current study enabled progress in refining more sustainable techniques to set leaf nutrient content. The present results can be used to guide future research aimed at improving the Vis-NIR technique to estimate leaf nutrients, so that this technique can be implemented at large scale in community service laboratories, in the near future.

Supplementary Materials: The following supporting information can be downloaded at: https://www.mdpi.com/article/10.3390/horticulturae12030296/s1, Table S1: average values of pH, Ca^{2+}, $Mg^{2+,}$ Al^{3+}, $H^+ + Al^{3+}$, Saturation (Al^{3+}, Ca^{2+}+Mg^{2+}+K^+), SMP index, MO, clay, P-Mehlich, CTC_{pH7}, CTC_{effect}, Cu^{2+}, Fe^{2+}, Mn^{2+} and Zn^{2+} from 42 soil samples collected in *Pinto Bandeira* (cultivar 'PS') and 59 samples collected in *Pelotas* (cultivar 'Maciel' and 'Granada'). Table S2: values of critical levels (CL) and sufficiency ranges (SR) of nutrients in leaves for peach cultivation—cultivars 'PS. 'Maciel' and 'Granada' in Southern Brazil. Figure S1: flowchart of steps taken to organize the LSL, prediction models' calibration and validation for the N, P, K, Ca, Mg, S, B, Cu, Fe, Mn and Zn content in the leaves of peach trees grown in *Pinto Bandeira* and *Pelotas* regions. Figure S2: association between principal component 1 (PC1) and principal component 2 (PC2) recorded for leaf nutrient contents, and observed reflectance for peach cultivars grown in two regions in Southern Brazil. Triangles represent *Pinto Bandeira* regions, and circles represent *Pelotas*.

Author Contributions: Conceptualization, J.H., J.M.M.-B., G.B. and F.J.K.M.; methodology, J.H., J.M.M.-B., G.B., E.Z.C., E.D.A., J.A.T.P., N.A., G.N., R.N. and F.J.K.M.; validation, J.H., J.M.M.-B., E.Z.C., E.D.A., J.A.T.P., N.A., G.N. and R.N.; resources, J.M.M.-B., G.B. and F.J.K.M.; data curation, J.H., J.M.M.-B., E.Z.C., E.D.A., J.A.T.P. and N.A.; writing—original draft preparation, J.H., J.M.M.-B. and F.J.K.M.; writing—review and editing, J.H., J.M.M.-B., G.B., T.T., W.N. and F.J.K.M.; visualization, J.H., J.M.M.-B., E.Z.C., E.D.A., J.A.T.P., N.A., G.N. and R.N.; supervision, J.M.M.-B., G.B. and F.J.K.M.; project administration, J.M.M.-B.; funding acquisition, J.M.M.-B., G.B. and F.J.K.M. All authors have read and agreed to the published version of the manuscript.

Funding: This study was funded by the Brazilian Federal Agency for Support and Evaluation of Graduate Education (CAPES), Financial Code 001, and also by the National Council of Scientific and Technological Development (CNPq) (term of grant 306146/2023-1) and the Foundation for Research Support of the State of *Rio Grande do Sul* (FAPERGS) (term of grant 21/2551-0001920-4).

Data Availability Statement: The original contributions presented in this study are included in the article/supplementary material. Further inquiries can be directed to the corresponding author(s).

Acknowledgments: The authors acknowledge *ASPROFRUTA* and *Embrapa Clima Temperado*, and the producers from the regions of *Pinto Bandeira* and *Pelotas* who welcomed us and made their orchards available for collection and carrying out this study.

Conflicts of Interest: The authors declare no conflicts of interest.

References

1. FAOSTAT—Food and Agriculture Organization of the United Nations: Crops and Livestock Products. 2023. Available online: https://www.fao.org/faostat/en/#data/QCL (accessed on 12 June 2025).
2. IBGE—Instituto Brasileiro de Geografia e Estatística. Produção de Pêssego: Brasil. Available online: https://ibge.gov.br/explica/producao-agropecuaria/pessego/br (accessed on 12 June 2025).
3. Diver City Times. Peach—Nectarine: Explore Definition, Production, Cultivation, Health Benefits, Nutrition, Structure, and Uses. Available online: https://divercitytimes.com/agriculture/crops-and-livestock/peaches-nectarines (accessed on 25 July 2025).

4. Rombolà, A.D.; Sorrenti, G.; Marodin, G.A.B.; de Pieri, A.Z.; Barca, E. Nutrição e manejo do solo em fruteiras de caroço em regiões de clima temperado. *Semin. Ciências Agrárias* **2012**, *33*, 639–654. https://doi.org/10.5433/1679-0359.2012v33n2p639.
5. Pascoa, R.N.M.J.; Lopo, M.; Teixeira dos Santos, C.A.; Graça, A.R.; Lopes, J.A. Exploratory study on vineyards soil mapping by visible/near-infrared spectroscopy of grapevine leaves. *Comput. Electron. Agric.* **2016**, *127*, 15–25. https://doi.org/10.1016/j.compag.2016.05.014.
6. Pascoa, R.N.M.J. In Situ Visible and Near-infrared Spectroscopy Applied to Vineyards as a Tool for Precision Viticulture. In *Comprehensive Analytical Chemistry*; Elsevier: Amsterdam, The Netherlands, 2018; Volume 80. https://doi.org/10.1016/bs.coac.2018.03.007.
7. Osco, L.P.; Ramos, A.P.M.; Pereira, D.R.; Moriya, É.A.S.; Imai, N.N.; Matsubara, E.T.; Estrabis, N.; de Souza, M.; Marcato, J., Jr.; Gonçalves, W.N.; et al. Predicting canopy nitrogen content in citrus-trees using random forest algorithm associated to spectral vegetation indices from UAV-Imagery. *Remote Sens.* **2019**, *11*, 2925. https://doi.org/10.3390/rs11242925.
8. Cuq, S.; Lemetter, V.; Kleiber, D.; Levasseur-Garcia, C. Assessing macro-element content in vine leaves and grape berries of *vitis vinifera* by using near-infrared spectroscopy and chemometrics. *Int. J. Environ. Anal. Chem.* **2019**, *100*, 1179–1195. https://doi.org/10.1080/03067319.2019.1648644.
9. Galvez-Sola, L.; García-Sánchez, F.; Pérez-Pérez, J.G.; Gimeno, V.; Navarro, J.M.; Moral, R.; Martínez-Nicolás, J.J.; Nieves, M. Rapid estimation of nutritional elements on citrus leaves by near infrared reflectance spectroscopy. *Front. Plant Sci.* **2015**, *6*, 571. https://doi.org/10.3389/fpls.2015.00571.
10. Corrêa, A.M.; Moura-Bueno, J.M.; Augusto Marconato, C.; da Silva Santos, M.; Marchezan, C.; Grando, D.L.; Tassinari, T.; Natale, W.; Rozane, D.E.; Brunetto, G. Combining Machine Learning and Vis-NIR Spectroscopy to Estimate Nutrients in Fruit Tree Leaves. *Horticulturae* **2026**, *12*, 108. https://doi.org/10.3390/horticulturae12010108.
11. Naibo, G.; José, J.F.B.D.S.; Zanotelli, C.C.; Pesini, G.; Lisboa, B.B.; Vargas, L.K.; Moura-Bueno, J.M.; Fior, C.S.; Tiecher, T. Near-infrared spectroscopy and machine learning to estimate the physical and chemical properties of soils cultivated with Ilex paraguariensis. *Environ. Technol. Innov.* **2025**, *40*, 104409. https://doi.org/10.1016/j.eti.2025.104409.
12. Naibo, G.; de São José, J.F.B.; Pesini, G.; Chemin, C.; Lisboa, B.; Kayser, L.; Abichequer, A.D.; Moura-Bueno, J.M.; Ramon, R.; Tiecher, T. Combining mid-infrared spectroscopy and machine learning to estimate nutrient content in plant tissues of yerba mate (*Ilex paraguariensis* A. St. Hil.). *J. Food Compos. Anal.* **2024**, *128*, 106008. https://doi.org/10.1016/j.jfca.2024.106008.
13. Zhu, G.; Wang, Q.; Zhang, S.; Guo, T.; Liu, S.; Lu, J. A meta-analysis of crop leaf nitrogen, phosphorus and potassium content estimation based on hyperspectral and multispectral remote sensing techniques. *Field Crops Res.* **2025**, *329*, 109961. https://doi.org/10.1016/j.fcr.2025.109961.
14. Bellon-Maurel, V.; Fernandez-Ahumada, E.; Palagos, B.; Roger, J.M.; McBratney, A. Critical review of chemometric indicators commonly used for assessing the quality of the prediction of soil attributes by NIR spectroscopy. *Trends Anal. Chem.* **2010**, *29*, 1073–1081. https://doi.org/10.1016/j.trac.2010.05.006.
15. Azadnia, R.; Rajabipour, A.; Jamshidi, B.; Omid, M. New approach for rapid estimation of leaf nitrogen, phosphorus, and potassium contents in apple-trees using Vis/NIR spectroscopy based on wavelength selection coupled with machine learning. *Comput. Electron. Agric.* **2023**, *207*, 107746. https://doi.org/10.1016/j.compag.2023.107746.
16. Flores, C.A.; Mandelli, F.; Falcade, I.; Tonietto, J.; Salton, M.A.; Zanus, M.C. Vinhos de Pinto Bandeira: Características de Identificação Regional para uma Indicação Geográfica. Circular técnica 55, Embrapa Uva e Vinho 2005, Bento Gonçalves, RS, 1-11. Available online: https://www.infoteca.cnptia.embrapa.br/infoteca/handle/doc/541424 (accessed on 10 Setember 2025).
17. Streck, E.V.; Kämpf, N.; Dalmolin, R.S.D.; Klamt, E.; Nascimento, P.C.; Giasson, E.; Pinto, L.F.S.; Flores, C.A.; Schneider, P. *Solos do Rio Grande do Sul*, 3rd ed.; rev. e ampl; Emater/RS: Porto Alegre, Brazil, 2018; 252p. Available online: https://www.bibliotecaagptea.org.br/agricultura/solos/livros/SOLOS%203%20EDICAO.pdf (accessed on 10 Setember 2025).
18. Brunetto, G.; Betemps, D.L.; de Paula, B.V.; Parent, L.E.; Melo, G.W.B.; Mayer, N.A. Proposição de níveis críticos de nutrientes através da metodologia CND em folhas de pessegueiros. In Proceedings of the XIII Reunião Sul Brasileira de Ciência do Solo: Conhecimento Aplicado ao Campo e à Cidade, Porto Alegre, Brazil, 26–27 November 2020; pp. 1–4. Available online: https://www.alice.cnptia.embrapa.br/alice/bitstream/doc/1128533/1/Proposicao-de-niveis-criticos-RSBCS-BRUNETTOetal-2020.pdf (accessed on 12 Setember 2025).
19. CQFS-RS/SC—Comissão de Química e Fertilidade do Solo RS e SC. *Manual de Calagem e Adubação para os Estados do Rio Grande do Sul e de Santa Catarina*, 11th ed.; Sociedade Brasileira de Ciência do Solo, Núcleo Regional Sul: Porto Alegre, Brazil, 2016; 376p. Available online: https://www.sbcs-nrs.org.br/docs/Manual_de_Calagem_e_Adubacao_para_os_Estados_do_RS_e_de_SC-2016.pdf (accessed on 12 Setember 2025).

20. Tedesco, M.J.; Gianello, C.; Bissani, C.A.; Bohnen, H.; Volkweiss, S.J. *Análise do solo, Planta e Outros Materiais*, 2nd ed.; Departamento de solo da UFRGS: Porto Alegre, Brazil, 1995; 174p. Available online: https://pt.scribd.com/document/362494561/Analise-de-solos-plantas-e-outros-materiais-Tedesco-et-al-1995-pdf (accessed on 12 Setember 2025).
21. EMBRAPA—Empresa Brasileira de Pesquisa Agropecuária. Métodos de Análise de Tecidos Vegetais Utilizados na Embrapa Solos. In *Circular Técnica N° 6*; Embrapa Solos: Rio de Janeiro, Brazil, 2000; 41p. Available online: https://www.infoteca.cnptia.embrapa.br/infoteca/bitstream/doc/337672/1/Metododeanalisedetecido.pdf (accessed on 12 Setember 2025).
22. EMBRAPA—Empresa Brasileira de Pesquisa Agropecuária. *Manual de Análises Químicas de Solos, Plantas e Fertilizantes*, 2nd ed.; rev. ampl.; Embrapa Informação Tecnológica: Brasília, Brazil, 2009; 627p. Available online: https://www.infoteca.cnptia.embrapa.br/infoteca/handle/doc/330496 (accessed on 12 Setember 2025).
23. Murphy, J.; Riley, J.P. A Modified single solution method for determination of phosphate in natural waters. *Anal. Chim. Acta* **1962**, *27*, 31–36. https://doi.org/10.1016/s0003-2670(00)88444-5.
24. Savitzky, A.; Golay, M.J.E. Smooting and Differentiation of Data by Simplified Least Squares Procedures. *Anal. Chem.* **1964**, *36*, 1627–1639. https://doi.org/10.1021/ac60214a047.
25. Rinnan, A.; Berg, F.V.; Engelsen, S.B. Review of the most common pre-processing techniques for near-infrared spectra. *Trends Anal. Chem.* **2009**, *28*, 1201–1222. https://doi.org/10.1016/j.trac.2009.07.007.
26. Stevens, A.; Ramirez-Lopes, L. An Introduction to the Prospectr Package. 2013. Available online: https://www.researchgate.net/publication/255941339_An_introduction_to_the_prospectr_package (accessed on 12 Setember 2025).
27. R Core Team, R: A Language and Environment for Statistical Computing. R Foundation for Statistical Computing. Available online: https://www.R-project.org/ (accessed on 5 Setember 2023).
28. Burnett, A.C.; Anderson, J.; Davidson, K.J.; Ely, K.S.; Lamour, J.; Li, Q.; Morrison, B.D.; Yang, D.; Rogers, A.; Serbin, S.P. A best-practice guide to predicting plant traits from leaf-level hyperspectral data using partial least squares regression. *J. Exp. Bot.* **2021**, *72*, 6175–6189. https://doi.org/10.1093/jxb/erab295.
29. Wold, S.; Sjöström, M.; Eriksson, L. PLS-regression: A basic tool of chemometrics. *Chemom. Intell. Lab. Syst.* **2001**, *58*, 109–130. https://doi.org/10.1016/S0169-7439(01)00155-1.
30. Kuhn, M. *The Caret Package*; R Foundation for Statistical Computing: Vienna, Austria, 2016.
31. Kennard, R.; Stone, L. Computer Aided Design of Experiments. *Technometrics* **1969**, *11*, 137–148. https://doi.org/10.1080/00401706.1969.10490666.
32. Brus, D.J.; Kempen, B.; Heuvelink, G.B.M. Sampling for validation of digital soil maps. *Eur. J. Soil Sci.* **2011**, *62*, 394–407. https://doi.org/10.1111/j.1365-2389.2011.01364.x.
33. Johnson, J.M.; Sila, A.; Senthilkumar, K.; Shepherd, K.D.; Saito, K. Application of infrared spectroscopy for estimation of concentrations of macro and micronutrients in rice in sub-Saharan Africa. *Field Crops Res.* **2021**, *270*, 108222. https://doi.org/10.1016/j.fcr.2021.108222.
34. Johnson, J.M.; Vandamme, E.; Senthilkumar, K.; Sila, A.; Shepherd, K.D.; Saito, K. Near-infrared, mid-infrared or combined diffuse reflectance spectroscopy for assessing soil fertility in rice fields in sub-Saharan Africa. *Geoderma* **2019**, *354*, 113840. https://doi.org/10.1016/j.geoderma.2019.06.043.
35. Chang, C.W.; Laird, D.A.; Mausbach, M.J.; Hurburgh, C.R. Near-infrared reflectance spectroscopy—Principal components regression analyses of soil properties. *Soil Sci. Soc. Am. J.* **2001**, *65*, 480–490. https://doi.org/10.2136/sssaj2001.652480x.
36. Veum, K.S.; Sudduth, K.A.; Kremer, R.J.; Kitchen, N.R. Estimating a soil quality index with VNIR reflectance spectroscopy. *Soil Sci. Soc. Am. J.* **2015**, *79*, 637–649. https://doi.org/10.2136/sssaj2014.09.0390.
37. Hindersmann, J.; Moura-Bueno, J.M.; Mallmann, F.J.K.; Bernardt, E.; Brunetto, G. Proposição de Níveis Críticos e Faixas de Suficiência de Nutrientes em Folhas de Pessegueiros da Cultivar 'PS 10711', Informes Técnicos 2025, CCR, UFSM. Available online: https://www.ufsm.br/app/uploads/sites/370/2025/07/Informe-Tecnico-CCR-Texto-Hindersmann-et-al.-2024_Final.pdf (accessed on 14 Setember 2025).
38. Moura-Bueno, J.M.; Dalmolin, R.S.D.; Horst-Heinen, T.Z.; Ten Caten, A.; Vasques, G.M.; Dotto, A.C.; Grunwald, S. When does stratification of a subtropical soil spectral library improve predictions of soil organic carbon content? *Sci. Total Environ.* **2020**, *737*, 139895. https://doi.org/10.1016/j.scitotenv.2020.139895.
39. Brunetto, G.; Melo, G.W.B.; Toselli, M.; Quartieri, M.; Tagliavini, M. The role of mineral nutrition on yields and fruit quality in grapevine, pear and apple. *Rev. Bras. De Frutic.* **2015**, *37*, 1089–1104. https://doi.org/10.1590/0100-2945-103/15.
40. Stefanello, L.O.; Schwalbert, R.; Schwalbert, R.A.; De Conti, L.; Kulmann, M.S.S.; Garlet, L.P.; Silveira, M.L.R.; Sautter, C.K.; Melo, G.W.B.; Rozane, D.E.; et al. Nitrogen supply method affects growth, yield and must composition of young grape vines (*Vitis vinifera* L. cv *Alicante Bouschet*) in southern Brazil. *Sci. Hortic.* **2020**, *261*, 108910. https://doi.org/10.1016/j.scienta.2019.108910.

41. Brunetto, G.; Nava, G.; Ambrosini, V.G.; Comin, J.J.; Kaminski, J. The pear tree response to phosphorus and potassium fertilization. *Rev. Bras. De Frutic.* **2015**, *37*, 507–516. https://doi.org/10.1590/0100-2945-027/14.
42. Zhou, Q.; Melgar, J.C. Tree Age Influences Nutrient Partitioning among Annually Removed Aboveground Organs of Peach. *HortScience* **2020**, *55*, 560–564. https://doi.org/10.21273/HORTSCI14731-19.
43. Korchagin, J.; Moterle, D.F.; Escosteguy, P.A.V.; Bortoluzzi, E.C. Distribution of copper and zinc fractions in a Regosol profile under centenary vineyard. *Environ. Earth Sci.* **2020**, *79*, 439. https://doi.org/10.1007/s12665-020-09209-7.
44. Mackie, K.A.; Müller, T.; Kandeler, E. Remediation of copper in vineyards—A mini review. *Environ. Pollut.* **2012**, *167*, 16–26. https://doi.org/10.1016/j.envpol.2012.03.023.
45. Bradl, H.B. Adsorption of heavy metal ions on soils and constituents. *J. Colloid Interface Sci.* **2004**, *277*, 1–18. https://doi.org/10.1016/j.jcis.2004.04.005.
46. Barreto, C.F.; Antunes, L.E.C.; Ferreira, L.V.; Navroski, R.; Benati, J.A.; Nava, G. Nitrogen fertilization and genotypes of peaches in high-density. *Rev. Bras. De Frutic.* **2020**, 42, e-629. https://doi.org/10.1590/0100-29452020629.
47. Lambers, H.; Brundrett, M.C.; Raven, J.A.; Hopper, S.D. Plant mineral nutrition in ancient landscapes: High plant species diversity on infertile soils is linked to functional diversity for nutritional strategies. *Plant Soil* **2010**, *334*, 11–30. https://doi.org/10.1007/s11104-010-0444-9.
48. Varmuza, K.; Filzmoser, P. *Introduction to Multivariate Statistical Analysis in Chemometrics*; CRC Press (Taylor & Francis): Boca Raton, FL, USA, 2009; 336p. https://doi.org/10.1201/9781420059496.
49. Petisco, C.; García-Criado, B.; Vázquez de Aldana, B.R.; Zabalgogeazcoa, I.; Mediavilla, S.; García-Ciudad, A. Use of near-infrared reflectance spectroscopy in predicting nitrogen, phosphorus and calcium contents in heterogeneous woody plant species. *Anal. Bioanal. Chem.* **2005**, *382*, 458–465. https://doi.org/10.1007/s00216-004-3046-7.
50. Curran, P.J. Remote sensing of foliar chemistry. *Remote Sens. Environ.* **1989**, *30*, 271–278. https://dx.doi.org/10.1016/0034-4257(89)90069-2
51. Jacquemoud, S.; Ustin, S.L. Leaf optical properties: A state of the art. *Remote Sens. Environ.* **2019**, *223*, 303–317. https://doi.org/10.1016/j.rse.2018.12.026.
52. Cullinan, C. B., Scomparin, A. N., Tagliavini, M., Janik, K. Dataset accompanying "Investigating the Limits of Spectroscopy for the Estimation of Foliar N and P in Apple": Hyperspectral reflectance, foliar nutrient concentrations and associated metadata. *Data in Brief*, **2025**, 112343. https://doi.org/10.1016/j.dib.2025.112343
53. Smith, J.A.; Jones, M.B. Spectral indices as indirect predictors of plant nutrient status: Strengths and limitations. *Remote Sens. Agric.* **2018**, *12*, 210–225.
54. Stenberg, B.; Viscarra Rossel, R.A.; Mouazen, A.M.; Wetterlind, J. Chapter Five—Visible and Near Infrared Spectroscopy in Soil Science. *Adv. Agron.* **2010**, *107*, 163–215. https://doi.org/10.1016/S0065-2113(10)07005-7.
55. Guerrero, C.; Viscarra Rossel, R.A.; Mouazen, A.M.; Wetterlind, J. Diffuse reflectance spectroscopy in soil science and land resource assessment. *Geoderma* **2016**, *158*, 83–97. https://doi.org/10.1016/j.geoderma.2016.03.004.
56. Bellon-Maurel, V.; McBratney, A. Near-infrared (NIR) and mid-infrared (MIR) spectroscopic techniques for assessing the amount of carbon stock in soils e Critical review and research perspectives. *Soil Biol. Biochem.* **2011**, *43*, 1398–1410. https://doi.org/10.1016/j.soilbio.2011.02.019.
57. Abenina, M.I.A.; Maja, J.M.; Cutulle, M.; Melgar, J.C.; Liu, H. Prediction of Potassium in Peach Leaves Using Hyperspectral Imaging and Multivariate Analysis. *AgriEngineering* **2022**, *4*, 400–413. https://doi.org/10.3390/agriengineering4020027.
58. Viscarra Rossel, R.A.; Behrens, T.; Ben-Dor, E.; Brown, D.J.; Demattê, J.A.M.; Shepherd, K.D.; Shi, Z.; Stenberg, B.; Stevens, A.; Adamchuk, V.; et al. A global spectral library to characterize the world's soil. *Earth-Sci. Rev.* **2016**, *155*, 198–230. https://doi.org/10.1016/j.earscirev.2016.01.012.
59. Silva, C.A.A.C.; Rizzo, R.; da Silva, M.A.; Caron, M.L.; Fiorio, P.R. Spatio-Temporal Generalization of VIS-NIR-SWIR Spectral Models for Nitrogen Prediction in Sugarcane Leaves. *Remote Sens.* **2024**, *16*, 4250. https://doi.org/10.3390/rs16224250.
60. Manzano, J.I.; Rodríguez-Febereiro, M.; Fandiño, M.; Vilanova, M.; Cancela, J.J. Spectroscopic analysis (UV-VIS-NIR) for predictive modeling of macro and micronutrients in grapevine leaves. *Smart Agric. Technol.* **2025**, *10*, 100812. https://doi.org/10.1016/j.atech.2025.100812.